

## BINARY COMPACT OBJECT COALESCENCE RATES: THE ROLE OF ELLIPTICAL GALAXIES

R. O'SHAUGHNESSY

Center for Gravitational Wave Physics, Penn State University, University Park, PA 16802, USA

V. KALOGERA

Northwestern University, Department of Physics and Astronomy, 2145 Sheridan Road, Evanston, IL 60208, USA

AND

KRZYSZTOF BELCZYNSKI<sup>1,2,3</sup>

<sup>1</sup> Los Alamos National Laboratory, CCS-2/ISR-1 Group

<sup>2</sup> Oppenheimer Fellow

<sup>3</sup> Astronomical Observatory, University of Warsaw, Al. Ujazdowskie 4, 00-478 Warsaw, Poland

*Draft version October 30, 2018*

### ABSTRACT

In this paper we estimate binary compact object merger detection rates for LIGO, including the potentially significant contribution from binaries that are produced in elliptical galaxies near the epoch of peak star formation. Specifically, we convolve hundreds of model realizations of elliptical- and spiral-galaxy population syntheses with a model for elliptical- and spiral-galaxy star formation history as a function of redshift. Our results favor local merger rate densities of  $4 \times 10^{-3} \text{ Mpc}^{-3} \text{ Myr}^{-1}$  for binary black holes (BH),  $3 \times 10^{-2} \text{ Mpc}^{-3} \text{ Myr}^{-1}$  for binary neutron stars (NS), and  $10^{-2} \text{ Mpc}^{-3} \text{ Myr}^{-1}$  for BH-NS binaries. We find that mergers in elliptical galaxies are a significant fraction of our total estimate for BH-BH and BH-NS detection rates; NS-NS detection rates are likely dominated by the contribution from spiral galaxies. Limiting attention to elliptical- plus only those spiral-galaxy models that reproduce current observations of Galactic NS-NS, we find slightly higher rates for NS-NS and largely similar ranges for BH-NS and BH-BH binaries. Assuming a detection signal-to-noise ratio threshold of 8 for a single detector (in practice as part of a network, to reduce its noise), corresponding to radii  $D_{\text{bns}}$  of the effective volume inside of which a single LIGO detector could observe the inspiral of two  $1.4M_{\odot}$  neutron stars of 14 Mpc and 197 Mpc, for initial and advanced LIGO, we find event rates of *any* merger type of  $2.9 \times 10^{-2} - 0.46$  and  $25 - 400$  per year (at 90% confidence level), respectively. We also find that the probability  $P_{\text{detect}}$  of detecting one or more mergers with this single detector can be approximated by (i)  $P_{\text{detect}} \simeq 0.4 + 0.5 \log(T/0.01 \text{ yr})$ , assuming  $D_{\text{bns}} = 197 \text{ Mpc}$  and it operates for  $T$  years, for  $T$  between 2 days and 0.1 yr; or by (ii)  $P_{\text{detect}} \simeq 0.5 + 1.5 \log(D_{\text{bns}}/32 \text{ Mpc})$ , for one year of operation and for  $D_{\text{bns}}$  between 20 and 70 Mpc.

*Subject headings:* Stars: Binaries: Close; Stars: Pulsars: General; Gravitational waves

### 1. INTRODUCTION

Over the last decade the question of the Galactic inspiral rate of binaries with two compact objects (neutron stars NS or black holes BH) has attracted attention primarily because of the development and planning of gravitational-wave interferometric detectors both on the Earth and in space (e.g., LIGO and GEO600, described in Abbott et al. (The LIGO Scientific Collaboration) (2003); Virgo, described at the Virgo project website [www.virgo.infn.it](http://www.virgo.infn.it); and LISA, at [lisa.nasa.gov](http://lisa.nasa.gov)). These rate estimates have been widely used in the assessment of gravitational inspiral detectability, given assumed instrument sensitivities. A number of different groups have calculated inspiral rates using population synthesis calculations, most commonly with Monte Carlo methods (Fryer et al. 1998; Portegies Zwart & Yungelson 1998; Brown & Bethe 1994; Fryer et al. 1999; Belczynski et al. 2002;

Voss & Tauris 2003). Such studies consider the complete formation history of double compact objects through long sequences of binary evolution phases, terminated by a gravitational-wave driven inspiral towards merger. Though less critical for studies of the Milky Way, contributions to the present-day merger rate per unit volume from early star formation has most often been ignored in merger rate calculations. Since long inspiral delays before merger are not sufficiently uncommon, even for double neutron stars, merger detection rate calculations should account for the full time history of star formation, including star formation in the early universe; see for example de Freitas Pacheco et al. (2006). Additionally, our current understanding of single and binary star evolution is incomplete. The many uncertainties have been parameterized and the resulting parameter space explored in some studies to determine the range of plausible results (see, e.g., Belczynski et al. 2008b), both by focusing narrowly on physically-motivated regions of parameter space as in Belczynski et al. (2008b) and by broadly exploring all plausible population synthesis simulations (see, e.g.,

O’Shaughnessy et al. 2008a, and references therein; henceforth denoted PS-GRB). Finally, by assigning equal prior likelihood to any population synthesis model, PS-GRB estimated the relative likelihood of any BH-NS or NS-NS merger rate.<sup>1</sup>

The population of binary black holes, however, behaves qualitatively differently from BH-NS or NS-NS binaries: (i) most of those that merge do so only after a few to several Gyr delay after their birth as binary stars; and (ii) those BH-BH binaries with merger times from 1 – 10 Gyr have masses quite different from the typical assumption of a  $10M_{\odot}$  BH; see Appendix. The rarity, long delay times, high masses and thus cosmologically significant detection horizons of binary black holes have already been discussed in the literature (see, e.g., Kulczycki et al. (2006) and references therein). However, population synthesis simulations extensive enough to contain a statistically meaningful binary black hole population come at a significant computational cost. Even with adequate population synthesis simulations, given the long-lived nature of the progenitors, BH-BH merger and detection rates depend critically on the earliest and least certain star formation rates. Certain exotic but not exceptionally uncommon binary evolution scenarios could lead to a “high rate tail” – a scenario with rare massive mergers, for example, that could plausibly produce a merger detection in the near future. In this paper we strive to understand what realistic scenarios could lead to a “high rate tail” that LIGO could detect or, conversely, constrain.

Given the technical challenges and significant uncertainties involved, only one paper (O’Shaughnessy et al. 2005) has previously estimated the relative likelihood of different BH-BH detection rate estimates expected from isolated binary star evolution, only for the Milky Way. In the present study we calculate the expected detection rate for LIGO while for the first time simultaneously including (i) all past star formation, particularly the overwhelming importance of elliptical galaxies; (ii) a large database of results that accounts for the dominant model uncertainties; and (iii) a careful treatment of the mass distribution of BH-BH binaries. Additionally, unlike previous analyses presenting distributions of merger rates, we have post-facto varied the birth binary fraction of stars from 100% to 15%; this addition allows us to better compare our results with the fiducial population synthesis model and BH-BH merger rates presented in Belczynski et al. (2007a). Finally, whereas previous comparisons relied essentially on confidence intervals (e.g., PS-GRB and O’Shaughnessy et al. (2008b), henceforth denoted PSC2), in this paper we generate true posterior distributions: each model is weighted by its relative conditional likelihood given observations of merging NS-NS binaries in the Milky Way.

To fully assess the *total* probability for a LIGO detection, rather than limit attention to BH-BH mergers we explore the rate at which all LIGO-detectable binaries (BH-BH, BH-NS, and NS-NS; henceforth collectively de-

noted as compact binary coalescences or CBCs) merge through gravitational wave emission. As the methods used to determine LIGO detection rates from population synthesis simulations are already extensively discussed in the literature (see, e.g. Bulik et al. 2004, and PS-GRB), our presentation only reviews those tools, emphasizing unique features of our present analysis (i.e., our methods to estimate BH-BH masses). Specifically, in § 2 we briefly review the ingredients that enter into an estimate of the gravitational wave detection rate for a short-ranged network ( $z_{max} \ll 1$ ). While the local universe is emphasized in the text, networks of advanced ground-based interferometers can detect optimally oriented BH-BH binaries with component masses  $M \simeq 10 - 15M_{\odot}$  at cosmologically significant distances  $z \geq 0.1$ . Merger rates on the past light cone of a detector become inhomogeneous (versus redshift) at this scale, simply because the star formation rate increases dramatically near  $z \simeq 1 - 2$  during the epoch of galaxy assembly. At these distances, the detection rate must be integrated over the mass distribution, the full networked orientation-dependent sensitivity, and redshift-dependent merger rate. This integral becomes increasingly sensitive to rare, high-mass events that can be seen in the ancient universe. Therefore, we generalize the short-range method described in § 2 to include all sources on the past light cone, to arbitrary redshift and with accurate orientation-dependent sensitivity. In § 3 we review the model for star formation in the universe adopted here. This experience is applied in § 4 (for BH-BH binaries) and § 5 (including NS-NS and BH-NS binaries too), where we review our population synthesis calculations; and explain what features of those calculations influence our predictions for the relative likelihood of a LIGO detection. These sections also describe Figure 7, which contains our predictions regarding initial and advanced LIGO detection rates. Finally, in § 5.2 we show how rate constraints from the observed sample of Milky Way NS-NS binaries affect the predictions for LIGO detection rates.

To summarize, by fully simulating the past history of the local universe, this paper develops models for the present-day detection rate of short-range ( $z \ll 1$ ) and long-range ( $z$  not much less than 1) gravitational-wave detectors. Our results are rate distributions, where each distribution includes some normalization uncertainties (star formation rate and fraction of stars born in binaries); certain population synthesis model parameters; and our simulation Monte Carlo uncertainty. Further, our Bayesian approach to model constraints surveys many key uncertainties that should be included, whatever the model family involved, when attempting to interpret upper limits or detections from pulsar populations and gravitational wave observatories. We believe our distributions represent the best predictions of a concrete, conservative model family that includes both elliptical and spiral star formation yet is also consistent with initial LIGO upper limits on CBC merger rates.

## 2. GRAVITATIONAL WAVE DETECTION

This section primarily reviews the final stage in any calculation of a LIGO detection rate: the connection between, on the one hand, the event rate per comoving volume  $\mathcal{R}$  and mass distribution  $p(m_1, m_2)$  of merging binaries and, on the other hand, the de-

<sup>1</sup> Previously, O’Shaughnessy et al. (2005, 2008b) estimated LIGO binary merger detection rates by extrapolating from the local Milky Way based on the blue light density in the nearby Universe. As we discuss here, their estimate is accurate for short distances and for binary merger progenitors that are not preferentially long-lived (i.e., the median delay between birth and merger is less than 1 Gyr).

tection rate  $R_D$  [Eq. (9)]. This relation depends critically on the range to which LIGO could observe each merger. A thorough discussion of the LIGO range requires careful review of data analysis strategies and interferometer network geometry, and remains substantially beyond the scope of this paper. For details see Abbott et al. (The LIGO Scientific Collaboration) (2008); Abbott et al. (The LIGO Scientific Collaboration) (2009) and references therein. For example, with modern multi-mass-region searches using inspiral templates, one essential effect is a merger detection threshold in SNR that changes with total binary mass, as the well-understood portions of detection templates grow shorter. In this paper, we adopt the customary set of approximations (described below) and ignore the errors they introduce.

The distance to which LIGO is sensitive can be calculated using the sensitivity of the detector (strictly, the strain noise spectral distribution  $S_h$ ), the masses of the inspiralling bodies, and the emitted waveform. [For simplicity, we will assume the black holes initially nonspinning.] Specifically, for a source with masses  $m_1$  and  $m_2$ , merging at a luminosity distance  $D$  (or equivalently at redshift  $z$ , or comoving distance  $r$ ) with a binary inclination  $\iota$  and a relative orientation to the detector given by  $\theta, \phi$  (the orientation on the sky) and  $\psi$  (a phase angle in the plane of the detector), the signal-to-noise seen by a matched-filter search in the LIGO data stream can be expressed relative to the strain noise spectrum of a single interferometer  $S_h$  and the Fourier transform  $\tilde{h}(f)$  of gravitational wave strain  $h(t)$  received at the detector by an arbitrarily oriented and located source by

$$\rho^2 = 4 \frac{w(\theta, \phi, \psi, \iota)^2}{D^2} \int_0^\infty df \frac{|r\tilde{h}(m_1(1+z), m_2(1+z), f)|^2}{S_h(f)} \quad (1)$$

using units with  $G = c = 1$ , the known dependence of planar-symmetry gravitational waves on angle, and a standard one-sided Fourier convention for  $\tilde{h}$  and  $S_h$  versus frequency  $f$ . The function  $w(\theta, \phi, \psi, \iota)$  takes values between 0 and 1 and completely encompasses the detector- and source-orientation dependent sensitivity for the most common sources, those that are dominated by  $l = m = 2$  quadrupole emission<sup>2</sup>

$$w(\theta, \phi, \psi, \iota) = \sqrt{F_+^2(1 + \cos^2 \iota)^2/4 + F_\times^2 \cos^2 \iota} \quad (2)$$

$$F_+ = \frac{1}{2}(1 + \cos^2 \theta) \cos 2\phi \cos 2\psi + \cos \theta \sin 2\phi \sin 2\psi \quad (3)$$

$$F_\times = -\frac{1}{2}(1 + \cos^2 \theta) \sin 2\phi \cos 2\psi + \cos \theta \cos 2\phi \sin 2\psi \quad (4)$$

To a rough approximation that depends on the data analysis strategy used and the amount of nongaussian noise present in the detector, a single LIGO interferometer can detect the gravitational wave signature of a merging binary if  $\rho > \rho_c$  (see, e.g., Abbott et al. (The LIGO Scientific Collaboration)

<sup>2</sup> Peak sensitivity is attained for a source directly overhead with orbital plane normal to the line of sight.

(2006, 2008), and references therein; henceforth we adopt  $\rho_c = 8$ ). For this reason, the previous expression for the signal to noise [Eq. (1)] is often re-expressed as

$$\rho = \rho_c w(\theta, \phi, \psi, \iota) \frac{D_H(m_1(1+z), m_2(1+z))}{D} \quad (5)$$

which, by comparison with Eq. (1), implicitly defines the *horizon distance*  $D_H$  – the maximum luminosity distance to which the detectors are sensitive – as a function of the redshifted masses  $m_1(1+z)$  and  $m_2(1+z)$  of the binary (see, e.g., Anderson et al. (2001), Finn & Chernoff (1993) and Flanagan & Hughes (1998) for a brief review of the theory underlying the direction-dependent LIGO sensitivity as well as for expressions that approximate  $D_H(m_1, m_2)$  for low-mass CBC binaries<sup>3</sup>).

More commonly used is the *volume-averaged distance*  $D_v$ , chosen so the volume of a sphere of radius  $D_v$  agrees with the average volume enclosed in a (Euclidean) detection surface:

$$D_v^3 = \frac{1}{4\pi} D_H^3 \int d\Omega \frac{d\psi}{\pi} \frac{d \cos \iota}{2} w^3 \simeq (D_H/2.26)^3 \quad (6)$$

The volume averaged distance is a meaningful measure of sensitivity only when the horizon range is much smaller than the Hubble scale.

A *network* of detectors can coherently add signals from each interferometer to increase the signal-to-noise  $\rho$  associated with each signal and by implication its reach. To a first approximation, ignoring small differences in sensitivity due to both their intrinsic differences and their orientations,<sup>4</sup> the combined SNR all interferometers is higher by roughly  $\sqrt{\sum_k L_k^2/L_1^2}$  where  $L_k$  is the length of the  $k$ th interferometer. For example, this factor is approximately  $g_N \simeq \sqrt{1 + 1 + 1/4} \simeq \sqrt{2.25}$  for the initial LIGO network, consisting of two 4 km and one 2 km interferometer; see Cutler & Flanagan (1994) for details on realistic multidetector beampatterns. However, in part because a network performs more trials of the same data streams (e.g., for each sky position) and is sensitive to both polarizations simultaneously, for the same false alarm rate the network detection threshold  $\rho_{c,net}$  is generally greater than the threshold  $\rho_c$  for the individual detectors; see for example Cutler & Flanagan (1994) and Buonanno et al. (2003) for a discussion in the case of gaussian noise. One can therefore speak of a single-interferometer ( $D_H$ ) and network ( $D_H^{(n)} \simeq g_N D_H(\rho_c/\rho_{c,net})$ ) horizon distance. Unfortunately, only expert analysis of real data can determine the sensitivity of real gravitational-wave networks, not the least because noise statistics (and

<sup>3</sup> A more thorough review of the orbital geometry and waveforms underlying the reach of a single-interferometer search for circularly inspiralling point particles can be found in Brown (2004) and (for the more complex case of spinning binaries) in Apostolatos et al. (1994); Buonanno et al. (2003). Additionally, Kopparapu et al. (2008) discusses how this orientation-dependent sensitivity influences the present-day LIGO search.

<sup>4</sup> The small bias ( $\simeq 10\%$ ) introduced by this approximation is much smaller than the characteristic uncertainties discussed later in this paper; see, for example, LIGO site location information in LIGO-T980044-10 (available at <http://admdbsrv.ligo.caltech.edu/dcc/>) and the LAL software documentation (available from <http://www.lsc-group.phys.uwm.edu/daswg/projects/lal.html>).

therefore  $\rho_{c,net}$ ) are highly detector- and even search-dependent. To avoid ambiguity and misleading approximations, we provide results for single, idealized interferometers assuming a detection threshold of  $\rho_c = 8$  (e.g., appropriate to gaussian noise). This reference sensitivity agrees with the customary sensitivity measure used in the LIGO coalescence search, a threshold of  $\rho_c = 8$  for a single detector as part of a network.<sup>5</sup> For sources in the local universe, without loss of generality the reader can scale our results to any realistic network and search.

For sources of sufficiently low mass ( $M_{tot} \lesssim 20M_\odot$ ), LIGO is primarily sensitive to less-relativistic and therefore better-understood phases of the spiral-in, allowing us to approximate the waveform by its Newtonian limit (Peters 1964). After considerable algebra (see, e.g. Flanagan & Hughes 1998; Cutler & Flanagan 1994), the signal-to-noise due to an optimally-oriented inspiral at comoving distance  $r$  (corresponding to a redshift  $z(r)$ ) can be related to the strain sensitivity  $S_h$  by

$$\rho^2 = \frac{5w^2[\mathcal{M}_c(1+z)]^{5/3}}{6\pi^{4/3}D^2} \int_0^\infty df \frac{f^{-7/3}}{S_h(f)} \quad (7)$$

where  $\mathcal{M}_c \equiv (m_1 m_2)^{3/5} / (m_1 + m_2)^{1/5}$  is the ‘‘chirp mass’’ of the binary. Based on this expression, individual interferometers in the initial<sup>6</sup>, and advanced<sup>7</sup> LIGO networks can see *low-mass* binaries ( $m_1 + m_2 \lesssim 40M_\odot$ )<sup>8</sup> out to a horizon (volume-averaged) distance

$$D_{H(v)} \simeq \mathcal{C}_{H(v)} (\mathcal{M}_c / 1.2M_\odot)^{5/6} \quad (8)$$

where  $\mathcal{C}_{H(v)} = 31(14)$  Mpc and  $\mathcal{C}_{H(v)} = 445(197)$  Mpc respectively. For clarity, the distance  $\mathcal{C}_v$  will henceforth be denoted  $D_{bns}$ , the volume-averaged distance to which a binary neutron star inspiral can be detected by a single interferometer as part of a network.

In terms of this horizon distance  $D_H$ , the intrinsic present-day rate of events per unit comoving volume  $\mathcal{R}(0)$ , and the chirp mass distribution of merging binaries  $p(\mathcal{M}_c)$ , the average rate of events with  $\rho > \rho_c$  occurring

<sup>5</sup> For the real LIGO interferometers, no single detector search at this threshold is possible; multi-detector coincidence is required to reduce the nongaussian background to roughly the level indicated (hence ‘‘as part of a network’’).

<sup>6</sup> We use a published LIGO S5 sensitivity (for the LHO interferometer, on March 13th, 2006), available at [http://www.ligo.caltech.edu/~jzweizig/distribution/LSC\\_Data](http://www.ligo.caltech.edu/~jzweizig/distribution/LSC_Data).

<sup>7</sup> We adopt an advanced LIGO noise curve from LIGO T0900288, available as ZERO\_DET\_high\_P.txt at <http://dcc.ligo.org/DocDB/0002/T0900288/002/>. This noise curve is taken from the GWINC program with Mode 1b parameters, as described in LIGO document LIGO-T070247-01-I: 125 W input laser power, 20% signal recycling mirror (SRM) transmissivity, and no detuning of the signal recycling cavity.

<sup>8</sup> For comparison, full strong-field numerical relativity waveforms suggest a single-interferometer initial LIGO horizon distance  $D_H$  to the most massive equal-mass binaries  $M \simeq 40$  that differs from the low-mass limit by 2%, multiplied by a factor of order unity; see Ajith et al. (2009). On the contrary, our limitation to *equal-mass, nonspinning* binaries introduces greater error: for binaries  $M \leq 16M_\odot$ , mass ratio corrections are roughly 4%, while black hole spin-dependent corrections are  $0.1J/m_{bh}^2$ , multiplied by a factor of order unity (if aligned). At the extreme, BH-NS binaries with strong spin-orbit misalignment and thus precession could be visible only out to  $0.5D_{Href}$ , multiplied by a factor of order unity, for  $D_{Href}$  the horizon distance to a comparable aligned binary. Such extreme uncertainties in range are less plausible, as isolated binary evolution models favor spin-orbit alignment.

in the nearby universe can be expressed as

$$R_D = \mathcal{R}(0) \int_{\frac{wD_H}{D} > 1} r^2 dr d\Omega \frac{d\psi}{\pi} \frac{d \cos \iota}{2} p(\mathcal{M}_c) d\mathcal{M}_c \quad (9)$$

$$= \mathcal{R}(0) \left[ \int d\mathcal{M}_c \frac{4\pi}{3} D_v(\mathcal{M}_c)^3 p(\mathcal{M}_c) \right]. \quad (10)$$

where the integral is taken over all detectable combinations of masses, orientation, and location. For low-mass binary mergers ( $M < 40M_\odot$ ), for which Eq. (8) applies, the chirp mass-weighted average simplifies to

$$R_D \simeq \mathcal{R}(0) \frac{4\pi(\mathcal{C}_v)^3}{3} \int p(\mathcal{M}_c) (\mathcal{M}_c / 1.2M_\odot)^{15/6} d\mathcal{M}_c \quad (11)$$

an expression that has been applied extensively in the literature to translate event rates per unit volume into LIGO detection rates (see, e.g. O’Shaughnessy et al. 2008b, and references therein).

### 2.1. Rates for advanced detectors

As the product of the present-day merger rate and an effective detection volume, the detection rate estimate Eq. (9) assumes a locally homogeneous and isotropic universe. Advanced detectors can see back to sky-position-dependent epochs with noticeably different star formation history ( $z > 0.1$ ). For advanced detectors, a more generic expression must be used, which integrates over the mass distribution, the redshift-dependent merger rate, and the orientation-dependent reach  $w$ .

For the purposes of this paper, we continue to assume the maximum luminosity distance to which a single interferometer can identify a merger in noise is well-described by the inspiral phase [Eq. 7]. To normalize our estimate, we adopt a single-interferometer advanced LIGO range of 445 Mpc. Based on the optimal range for a given chirp mass, each simulation’s the chirp mass distributions, and the single-interferometer beampattern  $w$  [Eq. 2], we determine the fraction of all mergers at redshift  $z$  that could be detected,  $P_{ok}(z)$ :

$$P_{ok}(z) = \int_{D(z) < wD_H} \frac{d\Omega}{4\pi} \frac{d\psi}{\pi} \frac{d \cos \iota}{2} d\mathcal{M}_c p(\mathcal{M}_c) \quad (12)$$

The overall single-interferometer detection rate is therefore the sum over the past light cone of the (redshifted) rate of mergers on it, times the fraction  $P_{ok}$  of mergers that could be detected:

$$R_D = \int dz \frac{dV}{dz} \frac{\mathcal{R}(t)}{1+z} P_{ok}(z) \quad (13)$$

For a maximum reach  $z \ll 1$ , these two expressions are equivalent to Eq. 7.

## 3. MULTICOMPONENT STAR FORMATION HISTORY

The LIGO detection rate depends on the mass distribution of merging binaries  $p(\mathcal{M}_c)$  and on the average rate of mergers per unit comoving volume,  $\mathcal{R}(t)$ . This rate, in turn, generally depends on the net contribution from multiple star-forming populations, a contribution that convolves the star formation rate in each component (the subject of the present section) with the rate at which each components’ star-forming gas yields CBC mergers

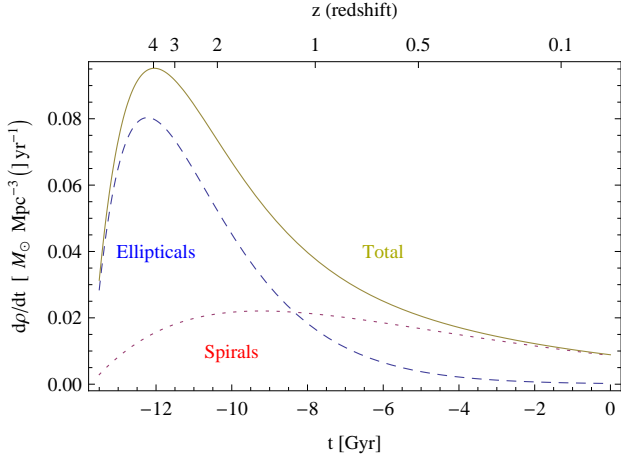


FIG. 1.— Star formation history of the universe used in this paper versus time, relative to the present day. Solid line: Net star formation history implied by Eq. (16). Dashed, dotted line: The star formation history due to elliptical and spiral components.

(the subject of § 4). More specifically, the merger rate density  $\mathcal{R}(t)$ , a quantity required to calculate the detection rate, is obtained from (i) the star formation rate in each component  $d\rho_C/dt$  where  $C$  indexes the different star-forming types,  $C = e$  for ellipticals and  $s$  for spirals, defined as the mass per unit comoving volume and time that forms as stars; (ii) the mass efficiency  $\lambda_C$  at which each type of CBC binaries form, defined as the total number of binaries that survive isolated evolution and form CBC binaries per unit star forming mass; and (iii) the probability distribution  $dP_{mC}/dt$  for merger events to occur after a delay time  $t$  after star formation, where  $dP_{mC}$  is the fraction of mergers occurring between  $t$  and  $t + dt$  after the progenitor binary forms at  $t = 0$ :

$$\mathcal{R}(t) = \sum_C \mathcal{R}_C(t) \quad (14)$$

$$\mathcal{R}_C(t) = \int_{-T}^t dt_b \lambda_C \frac{dP_{mC}}{dt}(t - t_b) \frac{d\rho_C}{dt}(t_b) \quad (15)$$

where the integration variable  $t_b$  is time at which  $\lambda d\rho$  binaries per unit volume are born. As first recognized by de Freitas Pacheco et al. (2006) and as demonstrated systematically in PS-GRB, a multicomponent star formation history that includes both elliptical and spiral galaxies must be applied when calculating present-day merger rates of double compact objects. Simply put, even though elliptical galaxies formed stars long ago,  $dP/dt$  decays slowly enough (roughly as  $1/t$ ; see, e.g., PS-GRB) that the high rate of star formation in the early universe can lead to a significant elliptical-galaxy-hosted merger rate density in the present-day universe. Because elliptical galaxies have distinctly different star forming conditions (e.g., metallicities) than present-day star-forming galaxies, models for stellar evolution in the universe should not require identical behavior in present-day solar-metallicity galaxies and in young ellipticals. A full multicomponent treatment is necessary. The first multicomponent star formation history was applied to predict BH-NS and NS-NS merger rates in PS-GRB; this paper employs the same framework and preferred star formation history, discussed below.

We adopt the two-component star formation history

model presented by Nagamine et al. (2006). This model consists of an early “elliptical” component and a fairly steady “spiral” component, with star formation rates given by

$$\dot{\rho} = \dot{\rho}_e + \dot{\rho}_s \quad (16)$$

$$\dot{\rho}_C = A_C(t/\tau_C)e^{-t/\tau_C} \quad (17)$$

where cosmological time  $t$  is measured starting from the beginning of the universe and where the two components decay timescales are  $\tau_{e,s} = 1.5$  and  $4.5$  Gyr, respectively (see Section 2 and Table 2 of Nagamine et al. 2006). These normalization constants  $A_{e,s} = 0.22, 0.06 M_\odot \text{yr}^{-1} \text{Mpc}^{-3}$  were chosen by Nagamine et al. (2006) so the integrated amount of elliptical and spiral star formation reproduce the present-day census of baryonic matter in ellipticals and spirals, allowing for a certain fraction of gas recycling between different generations of stars.<sup>9</sup> Figure 1 illustrates the star formation rates assumed by the model adopted here.

Each component forms stars in its own distinctive conditions, set by comparison with observations of the Milky Way and elliptical galaxies. We assume mass converted into stars in the fairly steady “spiral” component with solar metallicity and with a fixed high-mass initial mass function (IMF) power law [ $p = -2.7$  in the broken-power-law Kroupa IMF; see Kroupa & Weidner (2003)]. On the other hand, we assume stars born in the “elliptical” component are drawn from a broken power law IMF with high-mass index within  $p \in [-2.27, -2.06]$  and metallicity  $Z$  within  $0.56 < Z/Z_\odot < 1.5$ . These elliptical birth conditions agree with observations of both old ellipticals in the local universe (see Li et al. 2006, and references therein) as well as of young starburst clusters (see Fall et al. 2005; Zhang & Fall 1999, and references therein).

Since two independent stellar populations give birth to CBCs, the net detection rate  $R_D$  is the sum of the detection rate due to ellipticals and spirals. In particular, the probability distribution function for  $R_D$  is necessarily the convolution of the distribution functions for detection rates due to elliptical and spiral galaxies, respectively. Because of the many orders of magnitude uncertainty in merger rates and the need to smooth across relative errors, however, all our PDFs are stored and smoothed in a logarithmic representation, as  $p(\log R_D)$ ; see for example PS-GRB. For this reason, the convolution takes on an unusual form, involving an integral over the fraction  $f$  of the detection rate due to ellipticals (i.e.,  $f = R_{D,e}/R_D$ ). Using this variable to form the logarithmic convolution, the distribution for the net rate  $\log R_D$  can be calculated from the distributions for ellipticals and spirals ( $p_{e,s}$ ) as

$$\begin{aligned} p(\log R_D) &= \int_0^1 \frac{df}{f(1-f)\ln(10)} \\ &\times p_e(\log R_D + \log f) \\ &\times p_s(\log R_D + \log(1-f)) \\ &\equiv p_s \oplus p_e \end{aligned} \quad (18)$$

*Limitations of two-component model:* Our two component model implicitly adopts two extremely strong as-

<sup>9</sup> Our previous paper PS-GRB incorrectly listed a larger value  $A_s = 0.15 M_\odot \text{yr}^{-1} \text{Mpc}^{-3}$ .

assumptions: (i) that metallicity in each component does not significantly evolve with redshift and (ii) that all star-forming gas in each component is identical. While sufficient for most problems involving binary evolution, these approximations may be particularly ill-suited to determining the progenitors of gravitational wave detections. Very low metallicity environments could produce BHs with exceptionally high mass; also, the BH binary merger rate increases strongly with metallicity (see, e.g. Belczynski et al. 2009). Because of the long typical delay between progenitor birth and BH-BH merger, very low-metallicity environments in the early universe could contribute significantly to the present-day gravitational-wave detection rate Belczynski et al. (2008a). Even at present, low-metallicity environments exist often enough to potentially dominate the local merger rate (see, e.g., O’Shaughnessy et al. 2008c). For example, the nearby BH-BH progenitor binary IC 10 X-1 both lies in a low metallicity environment and suggests a high BH-BH detection rate for initial LIGO (0.5 yr, multiplied by a factor of order unity, strongly dependent on survey selection effects; see Bulik et al. (2008)).

Despite strong theoretical and observational evidence for a significant low-metallicity contribution, we have neither the confidence in the necessary astrophysical inputs (i.e., a redshift-dependent metallicity distribution) nor the required database of simulations to include these metallicity effects at this time. Further, unless initial LIGO detects BH-BH mergers, the peak detection rates cannot be significantly larger than what our model family predicts; see Figure 7. For this reason we continue to adopt the simple and conservative two-component mechanism outlined above.

*Relation to blue light density:* Previously, merger rate estimates for the Milky Way have been scaled up to the local universe, assuming mergers track blue light (see, e.g. Kopparapu et al. 2008, and references therein). As roughly speaking blue light traces star formation (see, e.g. Gallagher et al. 1984; Kennicutt 1998; O’Shaughnessy et al. 2008c), this extrapolation roughly agrees with our estimate for binary merger rates in spiral-like galaxies, with a suitable choice of normalization (i.e., star formation rate per unit blue light); see the conclusions for a detailed numerical comparison. O’Shaughnessy et al. (2008c) explains why blue light normalization was not adopted in this paper.

#### 4. CBC POPULATION SYNTHESIS MODELS

As outlined in § 2 and § 3 [see particularly Eqs. (9,15)], in order to estimate how often CBC binary mergers could be seen with gravitational-wave detectors we must know several features of the CBC population: (i) how many CBC binaries form from any given star forming mass (characterized by the mass efficiency  $\lambda$ ); (ii) how long these CBC binaries last between birth as stars and merger through gravitational wave emission (characterized by  $dP/dt$ ); and (iii) what masses these merging CBC binaries have (characterized by a probability distribution in chirp mass  $p(\mathcal{M}_c)$ ). In the absence of observations, these properties must be obtained from theoretical models of stellar and binary evolution. We study the formation of compact objects with the *StarTrack* population synthesis code, first developed by Belczynski et al. (2002) and recently significantly extended as described

in detail in Belczynski et al. (2008b). Since our understanding of the evolution of single and binary stars is incomplete, this code parameterizes several critical physical processes with a great many parameters ( $\sim 30$ ), many of which influence compact-object formation dramatically. In this specific study, in addition to the IMF and metallicity (which vary depending on whether a binary is born in an elliptical or spiral galaxy), seven parameters strongly influence compact object merger rates: the supernova kick distribution (modeled as the superposition of two independent Maxwellians, using three parameters: one parameter for the probability of drawing from each Maxwellian, and one to characterize the dispersion of each Maxwellian), the stellar wind strength, the common-envelope energy transfer efficiency, the fraction of angular momentum lost to infinity in phases of non-conservative mass transfer, and the relative distribution of masses in the binary. For this reason, following methods largely outlined in our previous work in PS-GRB and PSC2, we perform a broad *parameter study* to ensure all plausible population synthesis models have been explored. We include simulations of two different classes of star-forming conditions: “spiral” conditions, with  $Z = Z_\odot$  and a high-mass IMF slope of  $p = -2.7$ , and “elliptical” conditions, with a much flatter IMF slope  $p \simeq -2.3$  and a range of allowed metallicities  $0.56 < Z/Z_\odot < 1.5$ . Though we have performed thousands of simulations of these two types of conditions in the past (e.g., PS-GRB), to obtain better statistics on rare BH-BH events, we have constructed a new set of archives of  $N_S \equiv 282$  and  $N_E \equiv 206$  simulations of these two type of conditions, respectively. Within each set, we select parameters randomly according to the distributions described above; see the Appendix for more details.

The model database described above is statistically very similar to the database PS-GRB previously used to estimate NS-NS and BH-NS merger rates, with one critical exception: the simulations used here are extensive enough to have a statistically significant number of merging BH-BH binaries. Merging BH-BH binaries are a small fraction of the total BH-BH population and an exceedingly rare consequence of isolated binary evolution. For example, the number ( $n$ ) of BH-BH binaries in each of our simulations was always by construction 3000 and could be as high as  $\text{few} \times 10^5$  (see Figure 11). On the contrary, the number ( $m$ ) of *potentially merging* BH-BH binaries whose delay between formation and merger is less than 13.5 Gyr is typically 30, *multiplied by a factor of order unity*; despite our efforts, a spiral-galaxy simulation produced only one merging BH-BH binary (Figure 11). Further, among those few simulated binaries the most massive few can be seen to the greatest distance; thus, only a fraction of these  $m$  binaries significantly impact the average chirp mass  $\langle \mathcal{M}_c^{15/6} \rangle$  [Eq. (9)] calculated therefore our estimate of the detection rate. Given the small number statistics upon which we build our BH-BH detection rate predictions, we very carefully quantify and propagate uncertainties into our estimated BH-BH (and also BH-NS, NS-NS) detection rates.

##### 4.1. Model uncertainty and recent literature

Our simulations do not explore some known model uncertainties that could significantly increase the predicted merger rate. As noted previously, our star forming conditions involve only near-solar metallicity Bulik et al. (2008); Belczynski et al. (2008a, 2009). Additionally, we assumed that the common-envelope evolution of a Hertzsprung gap donor led to stellar merger, not a compact binary. However, as discussed in Belczynski et al. (2007a), the alternative and still plausible option will increase the BH-BH merger rate by  $\times 500$ . Finally, we assume binaries form through isolated evolution alone, not allowing for any enhancement in young globular proto-clusters; see, e.g., O’Shaughnessy et al. (2007b) and Sadowski et al. (2008). As mentioned previously, because these factors should *increase* the detection rate, our results are the predictions of a conservative model family.

Our simulations also do not self-consistently explore all model uncertainties corresponding that are comparable or smaller than the statistical simulation errors described extensively below. For example, as the StarTrack code has evolved over the extended assembly of our archive and this paper, our simulations differ somewhat from other contemporary papers that employ it. Notably, unlike Belczynski et al. (2007a), we adopt the full Bondi accretion rate during common-envelope evolution; by trapping more mass in the binary, this generally leads to larger detection rates.<sup>10</sup> Also, the StarTrack code does not yet fully explore all uncertainties in single star evolution, such as uncertainties in stellar radii (Fryer et al. 1999) and due to rotational effects (see, e.g., de Mink et al. (2009) Maeder & Meynet (2001) and references therein). Nor did we explore modifications to the recipes used by *StarTrack* for single and binary evolution. For example, StarTrack models orbital decay in common-envelope evolution with a single factor  $\alpha\lambda$ , though in principle  $\lambda$  differs between and can be calculated for different donor star configurations. For a supernova, the initial (pre-fallback) compact object remnant mass is estimated by tabulated estimates of the core mass; see Belczynski et al. (2008b). Compact remnants (post-fallback) more massive than  $2.5M_{\odot}$  are assumed to form black holes.

Finally, all of our results are sensitive to the total number of massive progenitor stars and our estimate for the high-mass IMF. While our computationally limited exploration cannot give an idealized, fully-marginalized theoretical prediction, our approach is extremely useful

<sup>10</sup> Though some black hole masses are influenced noticeably by a change in mass accretion, this change does not always lead to dramatic changes in BH-BH merger- and *detection* rates. For example, Belczynski et al. (2007a) provide a side-by-side comparison of the BH-BH merger rate for two different choices of the accretion (models A,B in their tables 2,3). They see less than a factor 2 change between these two extreme limits, much less than the typical variation due to the parameters we explore. [See also their Table 1 on BH-BH formation channels in these two models.] Given our limited computational resources, the fact that BH-BH detection rates are ubiquitously dominated by the highest-mass BH-BH binaries that merge (not the marginal BH-BH binaries where one formed through AIC), and recognizing that other model parameters (NS birth mass distribution) and physical inputs (metallicity distributions; systematic SFR normalization and model error) will perturb our predictions by a comparable amount to the factor of 2 mentioned above, we are comfortable with neglecting this parameter in this survey of BH-BH detection rates.

for the reverse problem: how this particular concrete, conservative model family can be tested against future gravitational wave observations.

#### 4.2. Properties of all CBC binaries

Though the calculation was applied only to BH-NS and NS-NS mergers, PS-GRB described how to calculate two of the three essential ingredients needed to calculate the CBC detection rate [Eqs. (9,15)]: (i) the number of CBC merger events per unit mass in progenitors (the mass efficiency  $\lambda_{C,\alpha}$ ); and (ii) the probability that given a CBC progenitor, a merger occurs between  $t$  and  $t+dt$  since the binary’s birth as two stars (the delay time distribution  $dP_{c,\alpha}/dt$ ). For example, as in PS-GRB we estimate the mass efficiency  $\lambda$  for forming a merging binary of type  $K$  (=BH-BH,BH-NS,NS-NS) from the number  $n$  of binary progenitors of  $K$  with

$$\lambda = \frac{n}{N} \frac{f_{cut}}{\langle M \rangle} \quad (20)$$

where  $N$  is the total number of binaries simulated, from which the  $n$  progenitors of  $K$  were drawn;  $\langle M \rangle$  is the average mass of all possible binary progenitors; and  $f_{cut}$  is a correction factor accounting for the great many very low mass binaries (i.e., with primary mass  $m_1 < m_c = 4M_{\odot}$ ) not included in our simulations at all. Expressions for both  $\langle M \rangle$  and  $f_{cut}$  in terms of population synthesis model parameters are provided in Eqs. (1-2) of O’Shaughnessy et al. (2007a). We also estimate the delay time distribution as before, by smoothing (in  $\log t$ ) the  $n$  simulated delays  $t$  between binary formation and merger; see particularly the Appendix of PS-GRB. Finally, though PS-GRB does not mention masses, we use precisely the same logarithmic smoothing technique to estimate  $dP/dM_c$  from a set of binaries; see our Appendix.

The procedures described above lead to very reliable results for NS-NS and BH-NS binaries, because many binaries  $n$  and even merging binaries  $m$  are present in each simulation. However, most simulations have only a few BH-BH binaries whose delays between birth and merger are less than the age of the universe. With so few merging binaries per simulation, statistical uncertainties would severely limit our ability to determine the physically relevant portion of delay time ( $dP/dt$ ) and chirp mass ( $p(M_c)dM_c$ ) distributions based on those binaries alone. However, since gravitational wave decay depends sensitively on the post-supernova orbital parameters of a newly-born BH-BH binary, the population of *merging* BH-BH binaries should be very similar to a population with marginally wider orbits but often dramatically longer decay timescales. For this reason, in this paper we will improve our statistics for  $dP/dt$  and  $p(M_c)$  by including nearly-merging binaries with delay times  $t$  between birth and merger less than a cutoff  $T = 10^5$  Myr, as justified by our studies in the Appendix.

#### 4.3. Varying the Binary Fraction

In our population synthesis simulations we systematically varied almost all parameters that could significantly impact the present-day merger rate. One parameter left unchanged in past studies, however, was the *binary fraction*  $f_b$ , defined as the fraction of stellar systems that

are binaries. Without loss of generality, our simulations assume *all* stars form in binaries. The merger rates per unit mass implied by a population with a lower binary fraction  $f_b$  can be related to the merger rates we calculate using

$$\mathcal{R}(t|f_b) = \mathcal{R}(t|f_b = 1) \frac{f_b(1 + \langle q \rangle)}{1 + f_b \langle q \rangle} \quad (21)$$

where  $\langle q \rangle = \langle m_2/m_1 \rangle$  is the average mass ratio of our initial stellar population and which is varied between population synthesis models. In particular, because the effect of this parameter trivially influences our rate predictions, we can *analytically* incorporate the influence of any prior assumptions regarding the binary fraction  $f_b$ .

The true initial binary fraction of stellar populations is not known; it is believed to be between  $f_{b,min} = 15\%$  and  $f_{b,max} = 100\%$  (Duquennoy & Mayor 1991). For this paper we will assume  $f_b$  could equally likely take on any value in this range. For any given population synthesis model, the binary fraction and mass ratio distribution multiplicatively influence the observed detection rate by a factor

$$X \equiv \frac{f_b(1 + \langle q \rangle)}{1 + f_b \langle q \rangle}. \quad (22)$$

which is distributed between  $X_{min}$  and  $X = 1$  (at  $f_b = 1$ ) according to

$$p(X)dX = \frac{1 + \langle q \rangle}{[\langle q \rangle(X - 1) - 1]^2} \frac{dX}{1 - f_{b,min}} \quad (23)$$

#### 4.4. Uncertainties and smoothing : Sampling errors

Roughly speaking, the relatively small numbers of merging binary black holes in any simulation ( $m \lesssim 100$ ) limit our ability to predict the overall detection rate  $\log R_D$  more accurately than  $1/\sqrt{m} \ln 10$ , because of inaccuracies in reproducing both the mass distribution  $dP/d\mathcal{M}_c$  and the delay time distribution  $dP/dt$ . Additionally, the relatively small number of *simulations* of elliptical and spiral galaxies  $N_{E,S} \simeq 300 - 400$  provides little chance of discovering high-rate models that are more rare than roughly  $1/N$ . To allow for these two errors, we must convolve each individual simulation's merger rate with kernels reflecting the poisson uncertainty introduced into each measurement by the limited number of samples. For simplicity, we approximate the relative error in  $\log N$  as normally distributed with standard deviation  $1/\sqrt{N} \ln 10$ . Translating this approximation into a PDF, instead of employing a poisson posterior distribution we adopt a simple gaussian kernel to describe the relative error in rate given  $m$  and  $N$  samples:

$$K_{sim} = K_o(\log R_D, 1/\sqrt{m} \ln 10) \quad (24)$$

$$K_{samp} = K_o(\log R_D, 1/\sqrt{N} \ln 10) \quad (25)$$

$$K_o(x, s) = \frac{1}{\sqrt{2\pi s^2}} \exp(-x^2/2s^2) \quad (26)$$

As noted above, a third uncertainty is the binary fraction, which we incorporate with the following kernel:

$$K_b(z, \langle q \rangle) \equiv \frac{10^z \ln 10}{1 - f_{b,min}} \frac{1 + \langle q \rangle}{[\langle q \rangle(10^z - 1) - 1]^2} \quad (27)$$

for  $\log 0.15 < z < 0$ . These terms capture the most significant simulation-related sources of error. We have

also explored and included several other potential sources of error, including (i) calibration uncertainty in the detector or mismatch in the waveform model (small, typically 10%, multiplied by a factor of order unity)<sup>11</sup>; (ii) uncertainty in the overall star formation history (a factor roughly 2) and in the relative proportions of elliptical and spiral galaxies (roughly 10%); and (iii) additional sampling errors introduced by the sensitivity of the chirp mass average to a few high-mass binaries ( $0.1/\sqrt{n_{eff}}/\ln 10$ , multiplied by a factor of order unity).

#### 4.5. Model prediction for CBC rate densities

To review, using the *StarTrack* population synthesis code, we have explored a representative sample of stellar evolution produced by elliptical galaxies ( $N_E = 206$ ) and spiral galaxies ( $N_S = 282$ ).<sup>12</sup> From these simulations, using the tools indicated in § 4 we carefully extracted their likely properties (e.g.,  $dP/dt$ ), which in turn we convolved with the star formation history of each of the two major components of the universe (§ 3) to generate a preferred present-day merger rate per unit volume  $\mathcal{R}_k(0)$  for each model  $k$ , for both elliptical and spiral star-forming conditions.

Though the set of model universe merger rates  $R_{(e,s)k}$  encompasses many of the most significant modeling uncertainties, to be more fully comprehensive and to arrive at a smooth PDF we convolve of the “model universe” merger rates  $R_{s,p}$  and  $R_{e,l}$  for  $p = 1, \dots, N_S$  and  $l = 1 \dots N_E$  with the uncertainty kernels and binary fraction kernel described previously assuming equal prior likelihood for each model (i.e.,  $P(E_l) = 1/N_E$  and  $P(S_p) = 1/N_S$ )

$$\bar{K} = (K_{samp} * K_{sim} * K_b) \quad (28)$$

$$p_e(\log R_e) = \sum_{l=1}^{N_E} P(E_l) \bar{K}(\log \frac{R_e}{R_{e,l}}) \quad (29)$$

$$p_s(\log R_s) = \sum_{p=1}^{N_S} P(S_p) \bar{K}(\log \frac{R_e}{R_{e,p}}) \quad (30)$$

$$p(\log R) = (p_e \oplus p_s) \quad (31)$$

Figure 2 shows all of the kernels  $\bar{K}$ . In Figure 3 the thin ( $p(\log R)$ ) and dashed ( $p_e(\log R)$ ) curves correspond precisely to the output of this procedure. The bottom right panel also shows our estimate for the *total* merger

<sup>11</sup> Calibration of the amplitude and phase relationships between different measured frequencies can significantly perturb results. The target calibration amplitude error usually cited is 10%, multiplied by a factor of order unity; see M. Landry (for the LIGO Scientific Collaboration) (2005) and Adhikari et al. (2003) for a detailed survey.

<sup>12</sup> We do not calculate BH-NS or NS-NS merger rates for all 206 elliptical or 282 spiral-galaxy simulations; see Table 1 (available in the online version of the Journal). Following the discussion in the Appendix and PS-GRB, we only evaluate BH-NS and NS-NS merger rates when they are adequately resolved ( $n$  large) and (to correct for the bias this introduces) adequately unbiased ( $nN$  large). Roughly 10% of simulations are not used when evaluating the NS-NS or BH-NS merger rate distribution. These models form merging BH-BH binaries much more efficiently than BH-NS or (occasionally) NS-NS binaries. As discussed in the Appendix, we expect observational constraints inevitably rule out the few spiral galaxy models involved.



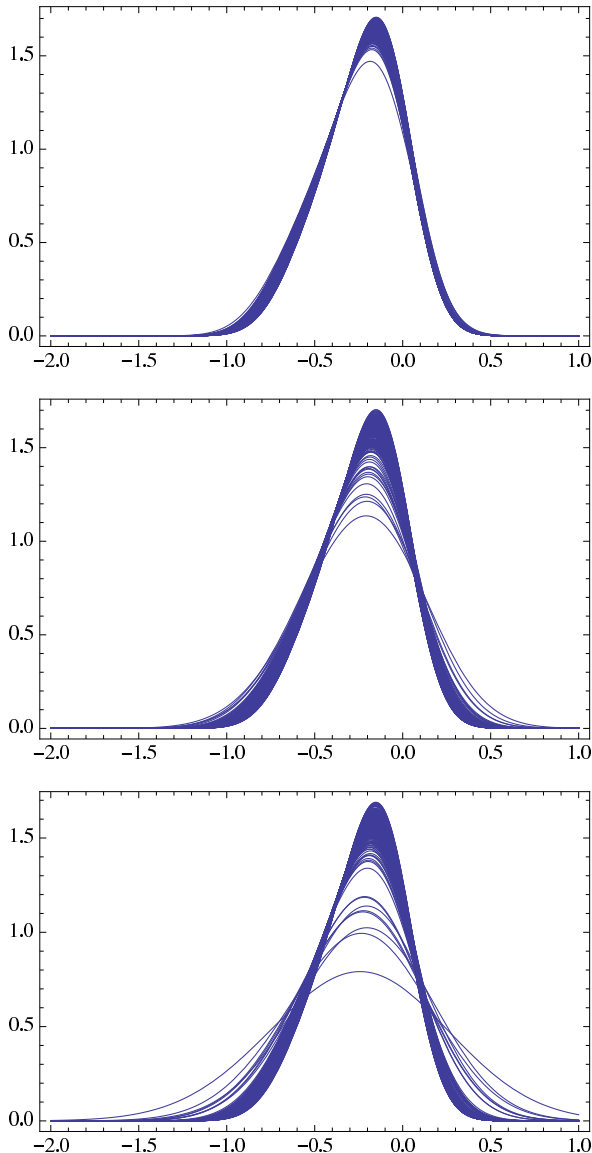


FIG. 2.— All of the kernels  $\bar{K}$  versus  $\log X$  used in this paper, for NS-NS (top panel), BH-NS (center panel), and BH-BH (bottom panel). As extremely many binaries are available in each simulation, the NS-NS simulations' uncertainties are dominated by the uncertainty in the binary fraction  $f_b$ . Because few BH-BH and occasionally BH-NS binaries are available in each simulation, however, the statistical uncertainty becomes significant.

rate distribution: a three-fold convolution<sup>13</sup>

$$p(\log R) = p_{BH-BH} \oplus p_{BH-NS} \oplus p_{NS-NS} \quad (32)$$

In the above we assume all simulated population synthesis models are equally plausible *a priori*. However, observations of single and binary pulsars significantly affect our perspective regarding the relative likelihood of different models. NS-NS merger rates derived from the observed sample are in fact typically higher than what most population models predict for the Milky Way. We adopt standard Bayesian methods to determine the posterior probability  $P(S_p|C)$  for a given spiral-galaxy model  $S_p$  ( $p = 1 \dots N_S$ )

$$P(S_p|C) \propto P(C|S_p)P(S_p) = P(C|S_p)/N_S \quad (33)$$

given the observational constraint  $C$  on the present-day spiral-galaxy contribution to the NS-NS merger rate implied by present-day observations of pulsars. We adopt as a constraint the requirement developed in PS-GRB from existing NS-pulsar observations, that the spiral-galaxy merger rate density of double neutron stars lie between 0.15 and 5.8  $\text{Myr}^{-1} \text{Mpc}^{-3}$  (90% confidence). The probability  $P(C|S_p)$  that the  $p$ th spiral-galaxy model predicts a rate consistent with observations of double neutron stars is found simply by integrating the PDF  $P(\log R|S_p)$  for the rate over the constraint interval<sup>14</sup>  $C = [0.15, 5.8] \text{Myr}^{-1} \text{Mpc}^{-3}$ . After renormalizing the probabilities  $P(C|S_p)$  into  $P(S_p|C)$  by requiring  $\sum_p P(S_p|C) = 1$ , we arrive at revised predictions for CBC merger rates for BH-BH, BH-NS, and NS-NS binaries as in Eqs. (29-31) but with conditional probabilities:

$$p_s(\log R_s|C) = \sum_{p=1}^{N_S} P(S_p|C) \bar{K}(\log \frac{R_s}{R_{s,p}}) \quad (34)$$

Convolving the constrained spiral rate density distribution  $p_s$  with the unconstrained elliptical density  $p_e$  leads to our best estimate for the present-day merger rate per unit volume, shown as the thick solid curve in Figure 3. Our best results favor merger rates between  $2 \times 10^{-3} - 0.04 \text{Mpc}^{-3} \text{Myr}^{-1}$  for BH-BH mergers (90%

<sup>13</sup> Strictly, the merger rate distribution function should be calculated by (i) finding the total merger rate predicted by each model (e.g.,  $R_e = R_{bbh} + R_{bhns} + R_{nnsns}$ ); (ii) centering an error kernel  $K$  on that rate, with  $n$  set by the total number of mergers of all types; and then (iii) convolving the elliptical and spiral distributions together as Eq. 31. The approach adopted in the text assumes the joint BH-BH, BH-NS, and NS-NS rate distribution is *uncorrelated*, even though weak correlations are apparent in Table 1 across our broad range of parameters (the table is available in the online version of the Journal). As described in §4.6, this assumption slightly biases us towards higher rates. On the contrary, the three-fold convolution *also* implicitly introduces independent binary fractions for BH-BH, BH-NS, and NS-NS binaries, biasing towards lower rates. Empirically, as can be confirmed using Table 1 this estimate for  $p(\log R)$  is in reasonable agreement with the summed calculation described above. Finally, since LIGO detection rates are ubiquitously dominated by the few most massive objects that merge – i.e., on  $p_{BH-BH}$  – the total *detection* rate does not depend sensitively on this order of evaluation issue.

<sup>14</sup> Strictly, we should calculate the Bayesian probability with some  $P(\log R|O)$  that describes the merger rate in spirals implied by PSR-NS binaries in the Milky Way and uncertainties in the star formation rate density of Milky Way galaxies. Our choice of a confidence interval based on broadening the the 90% confidence limit for PSR-NS binaries simplifies the discussion.

confidence),  $0.01 - 0.28 \text{ Mpc}^{-3} \text{ Myr}^{-1}$  for BH-NS mergers, and  $0.11 - 1.7 \text{ Mpc}^{-3} \text{ Myr}^{-1}$  for NS-NS mergers.

Our previous papers have similarly constrained binary evolution in the Milky Way (PSC2) and in the population of spiral galaxies (PS-GRB). Both interpret observations as much tighter constraints than we do here, because these papers did not allow for error (e.g., in each simulation’s prediction and, for the predictions per unit volume, in the star formation history of the universe). Our bayesian constraints are significantly less restrictive. Nonetheless, as seen in Figure 4 the top spiral galaxy models (90%) have a kick velocity distribution roughly consistent with pulsar observations, similar to that recovered in PSC2 (their Figure 5). Our predictions for the posterior NS-NS merger rate are conservative for another, technical reason: we implement the binary fraction as an *uncertainty* rather than a parameter. We therefore cannot rule out the lowest low binary fractions we allow ( $f_b = 0.15$ ) in other spiral galaxies, even though a comparison between binary pulsars in the Milky Way and our model database disfavors such low values.

#### 4.6. Discussion

*Two-component universe rarely gives low rates:* The probability we assign to very low rates depends sensitively on our implicit assumption that elliptical and spiral galaxy star forming conditions are *uncorrelated*. The convolution  $p_e \oplus p_s$  [Eq. (18)] assigns little probability below the sum of the median elliptical and median spiral merger rate; see, e.g., Figure 6. On the contrary, if all galaxies have the same undetermined star forming conditions, then the relevant merger rate distribution

$$p(\log R) = \sum_p P(S_p) \bar{K} \left( \log \frac{R}{R_{e,p} + R_{s,p}} \right) \quad (35)$$

assigns more probability to the lowest rates; see, e.g., the bottom panel of Figure 6. Adopting this implicit prior – identical star forming conditions in elliptical and spiral galaxies – leads to minimum plausible total BH-BH, BH-NS, and NS-NS merger rates  $\mathcal{R}_{5\%}$  roughly 2.4, 7, and 3.3 times larger than  $\max(\mathcal{R}_{e,5\%}, \mathcal{R}_{s,5\%})$ , where  $\mathcal{R}_{e,5\%}$  is the 5% probability elliptical-galaxy merger rate and similarly; compare, e.g., the top panel of Figure 6 with Figure 3.

*Ellipticals have different star formation?:* As in de Freitas Pacheco et al. (2006), our fiducial calculations suggest that elliptical galaxies gave birth to a significant fraction of all present-day compact object mergers, particularly BH-BH mergers [Figure 3]. Our results inevitably depend on the amount of and conditions for star formation in elliptical versus spiral galaxies. On the one hand, we assume most ancient star formation has occurred in ellipticals. On the other hand, the Salpeter-like IMFs ( $p \simeq -2.3$ ) adopted for elliptical galaxies produce compact object binaries much more efficiently than the much steeper high mass slope ( $p = -2.7$ ) adopted for spiral galaxies.<sup>15</sup> To quantify the impact of each factor

<sup>15</sup> The steep IMF for spiral-like galaxies is motivated by Kroupa & Weidner (2003), which theoretically examined the effective single-star IMF produced from continuous formation of open clusters. For elliptical galaxies, lacking any definitive suggestion that a similar throttled star formation process occurs, we adopt a standard Salpeter IMF.

separately, in Figure 5 we compare our fiducial BH-BH and NS-NS merger rate distributions (thick solid curves) with predictions based on *only* spiral or elliptical star forming conditions. Specifically, each new distribution still follows from Eq. (15) [to get  $\mathcal{R} = \mathcal{R}_s$  from our set of spiral-galaxy simulations] and Eq. (30) [to create a PDF, based on  $\mathcal{R}$ , an error kernel, and probability  $P(S)$ ]. These comparisons allow us to determine the relative impact that three key factors have on our predicted results: (i) significantly increasing ancient star formation; (ii) requiring ancient star formation produce high mass stars more efficiently than present-day star formation; and (iii) adopting independent binary evolution models for elliptical and spiral galaxies. First, both in distribution and on a model-by-model basis, the total compact object merger rate due to nearly-steady star formation (blue curves, which adopt the “spiral” star formation rate  $\dot{\rho} = \dot{\rho}_s$ ) is less than the amount due to all past star formation history (red curves, which adopt  $\dot{\rho} = \dot{\rho}_e + \dot{\rho}_s$ ) only by a simulation-dependent factor between 1.15-1.3 for NS-NS and between 1.5-2 for BH-BH binaries.<sup>16</sup> Second, on a model-by-model<sup>17</sup> and distribution basis, provided the same amount of star formation our elliptical galaxy models produce merging binaries roughly 1 (NS-NS) or 1 – 10 (BH-BH) times more frequently than spiral-only star forming conditions (both multiplied by factors of order unity), entirely due to their shallower IMF and broader metallicity distribution; compare the red and green curves in Figure 5. Third, though ellipticals produce merging binaries more efficiently per unit mass, fairly few BH-NS and NS-NS binaries remain to merge after such a long delay ( $dP/dt \propto 1/t$ ). For BH-NS and NS-NS binaries, elliptical galaxies’ present-day merger rate balances two positive factors – very efficient compact binary formation (e.g.,  $\sim 3$  times higher, based on the IMFs) combined with a high rate of early star formation ( $\sim 10$  times higher) – against an  $\sim 30$  lower merger rate  $dP/dt$  via a few Gyr vs  $\sim 100 \text{ Myr}$  typical delay; see the discussion in PS-GRB. For BH-NS and NS-NS binaries, this balance roughly leads to comparable merger rates in elliptical and spiral galaxies.<sup>18</sup> To summarize, our fiducial unconstrained predictions differ from previous predictions based on steady, spiral-galaxy star formation by three factors: (i) the addition of ancient star formation, increasing the overall merger rate above steady spiral-only by a factor 1.15 – 1.3 for NS-NS and 1.5 – 2 for BH-BH; (ii) the conversion of ancient star forming conditions from spiral-like to elliptical, increasing the total *present-day* merger rate by a factor of order unity for BH-NS and NS-NS binaries; and (iii) the assumption that elliptical and spiral star forming conditions are independent, biasing against low total merger rates.<sup>19</sup>

<sup>16</sup> The merger rates per unit volume are higher than an extrapolation of the Milky Way’s rate to a volume density by a factor of roughly  $[\int dP_{m,NS-NS}/dt \dot{\rho}(t)]/\dot{\rho}(0) P_{m,NS-NS} (< 13 \text{ Myr})$ .

<sup>17</sup> Though not used or provided here, we have compared several pairs of binary evolution models which differ only in their IMF and metallicity.

<sup>18</sup> In fact, the spiral NS-NS merger rate is significantly higher than the elliptical NS-NS rate, due to the existence of a population of ultracompact binaries not well described by this argument.

<sup>19</sup> Additionally, we apply observational constraints only to spiral galaxies, insuring the retention of elliptical galaxy models with the highest BH-BH formation rates. As discussed in §5.2, the spiral-

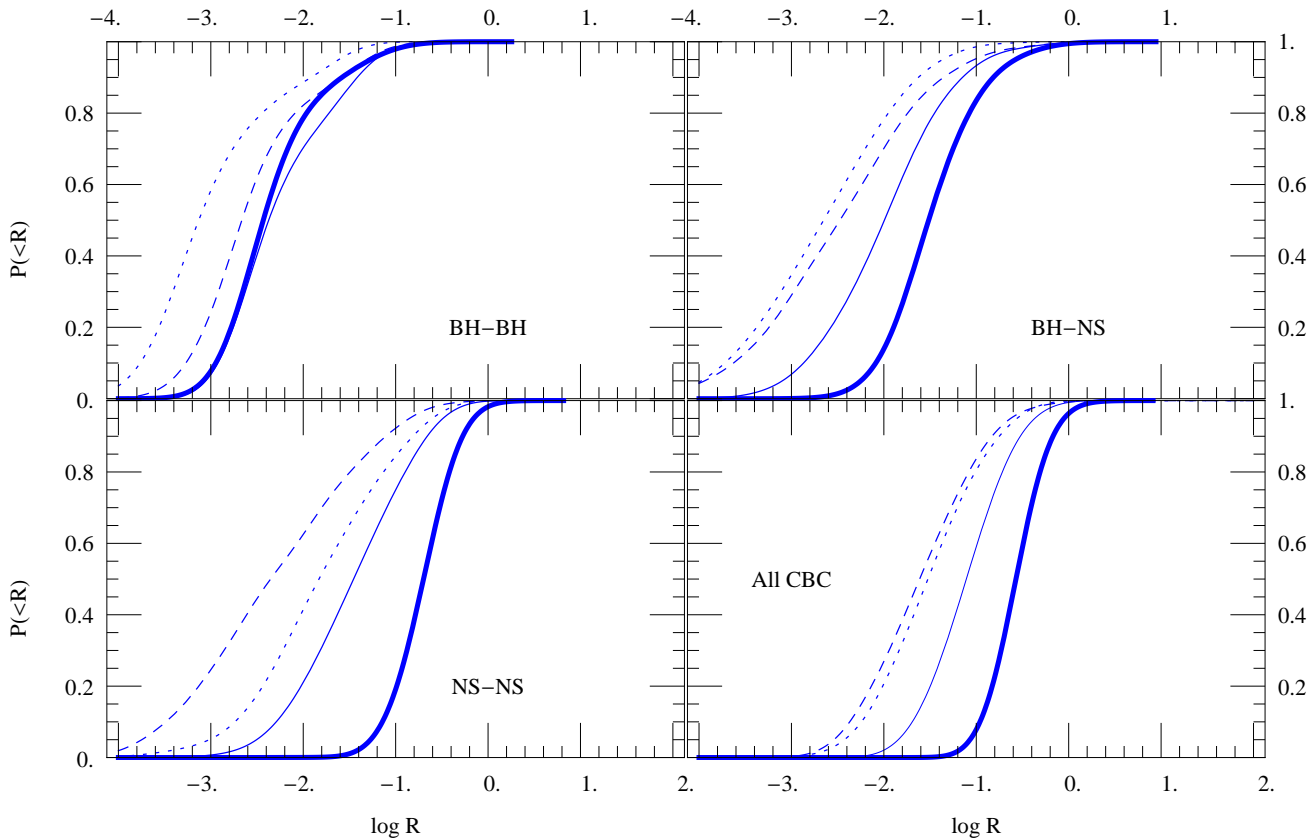


FIG. 3.— Cumulative probability  $P(< \log R)$  of various merger rates per unit volume (units  $\text{Mpc}^{-3} \text{Myr}^{-1}$ ), without (thin) and with (thick) requiring consistency with the binary pulsar population in the Milky Way. These distributions incorporate uncertainty in the initial binary fraction, the unknown population synthesis model parameters, and statistical errors implied by the limited size of our simulations. For comparison, the dashed lines show the contribution from *ellipticals only*; the dotted lines show the contribution from spiral galaxies *without requiring consistency* with the Milky Way.

*Ellipticals “dominate” BH-BH rate:* Adopting the same binary evolution model but different star formation histories, elliptical galaxies usually produce more merging BH-BH binaries at present than spiral galaxies. In this sense, the elliptical galaxy BH-BH merger and detection rates “dominate” the total merger rate. However, some elliptical galaxy models do yield lower merger rates than some spiral galaxy models; neither *ubiquitously* dominates. For example, Figure 6 suggests that low but plausible total BH-NS merger rates require more mergers in spirals than ellipticals; high but plausible merger rates require the opposite.

*Binary evolution priors:* Our predictions depend on the relative likelihood of different binary evolution model parameters. To facilitate comparison with PSC2 and to avoid omitting any vital region of parameter space, we allow and treat as equally plausible a wide parameter range, including extremely large (and empirically implausible) supernova kick magnitudes  $v_{kick} \simeq 1000 \text{ km/s}$ . The reader can reproduce our results or explore alternative assumptions by reweighting the data provided in Table 1, available in the online version of the Journal.

galaxy models with frequent-enough NS-NS mergers generally have  $\alpha\lambda$  not too small. Very inefficient common envelope evolution is required to produce the highest BH-BH merger rates.

*Binary evolution parameters:* Finally, as outlined in § 4.1, we fix a number of assumptions which can dramatically influence merger and even detection rates. For example, the maximum NS mass  $m_{+NS}$  completely determines the nature of final compact binaries, as it subdivides a roughly  $m_{+NS}$ -independent mass distribution into three regions: NS-NS, BH-NS, and BH-BH. Evidently the individual *component* merger rates depend sensitively on  $m_{+NS}$ . However, as relevant gravitational wave interferometers cannot easily distinguish between two compact objects of comparable mass  $1M_{\odot} < m < 3M_{\odot}$ , the *overall detection rate* described later depends only weakly on  $m_{+NS}$ . Similarly, while the neutron star birth mass distribution can influence the relative proportions of each type, as well as the observable pulsar binary mass distribution, our results should not depend significantly on the amount distribution of masses.

Several other binary evolution parameters not explored here have previously been shown to influence merger rates significantly, albeit much less significantly than the parameters we explored here. First, as noted previously in §4.1, we adopt the full Bondi-Hoyle accretion rate onto black holes in common envelope, rather than the smaller rates suggested by recent hydrodynamical simulations; cf. Belczynski et al. (2007a,b). A smaller

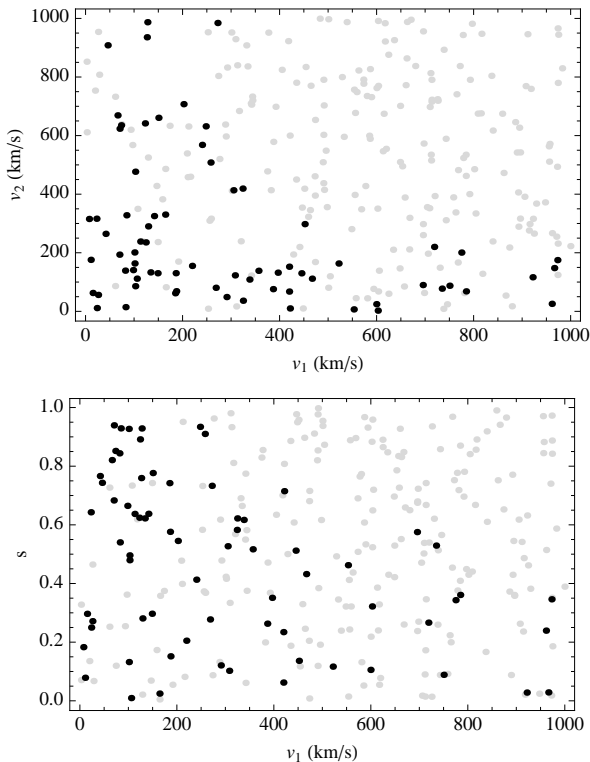


FIG. 4.— Constrained population synthesis parameters for spiral galaxies: compare to the top right and bottom left panels of Figure 5 of PSC2. In each panel, dark points are included when the corresponding model’s posterior probability  $P(S_p|C)$  is among the top 90%; gray points are shown for all other 282 spiral galaxy simulations.

mass accretion rate, if adopted, would reduce the incidence of accretion induced collapse, marginally changing the proportions of BH-BH, BH-NS, and NS-NS binaries; marginally lower the masses of some merging binaries; increasing the factor by which common envelope evolution tightens orbits; and generally change merger and detection rates by a small factor compared with the overall range considered [Footnote 10]. Second, we examined only isotropic kick distributions. Several authors have suggested spin-kick alignment on theoretical and empirical grounds; see, e.g., Kalogera et al. (2008), Kuranov et al. (2009) Wang et al. (2007) and references therein. As the same mass transfer that brings binaries close enough to merge also aligns their spins and orbit before the second supernova, polar kicks are particularly efficient at disrupting binaries; see Postnov & Kuranov (2008). Though polar kicks would dramatically transform our predictions, the observed PSR-NS merger rate in the Milky Way not only corresponds to a *high*, not low rate<sup>20</sup> but also implies model supernova kick magnitudes comparable to observed pulsar proper motion velocities [PSC2, as well as our Figure 4]. Third, we adopt a specific model for mass loss in massive stars; by changing the evolution of massive progenitors, alternate stellar wind models can dramatically modify merger rates (cf. Belczynski et al. (2008a)). Fourth, we adopt a sin-

<sup>20</sup> While the range of predicted Milky Way NS-NS merger rates depends on the adopted IMF, even a standard Salpeter IMF leads to a range of predictions that intersects PSR-NS observations only for high rates.

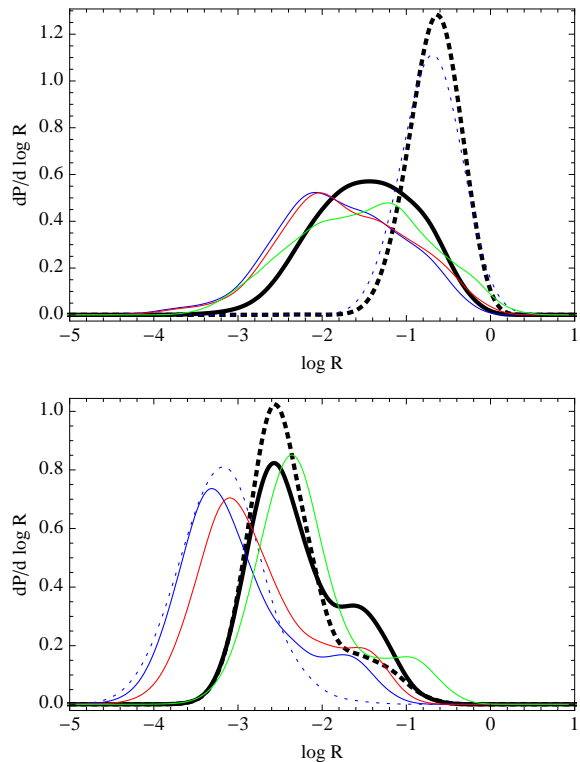


FIG. 5.— Relative likelihood of present-day merger rates  $R$  for NS-NS binaries (top panel) and BH-BH binaries (bottom panel) given five assumptions: (1) only nearly steady spiral galaxy star formation produces merging binaries (blue); (2) all galaxies form stars like spiral galaxies (red); (3) all galaxies form stars like elliptical galaxies (green); (4) like (1), but using only models that reproduce the present-day Milky Way merger rate (blue, dotted); (5) like (2), similarly (red, dotted). For comparison, the thick black curves shows the fiducial total BH-BH and NS-NS merger rate (solid curve includes all spiral models; dotted curve only models that reproduce the present-day Milky Way).

gle, time-independent metallicity for each type of star forming region. Binary merger rates can depend sensitively on metallicity, particularly through metallicity-dependent stellar winds (Belczynski et al. 2008a). A future publication will explore the latter two issues in more detail.

*Advanced detectors and redshift-dependent mass evolution:* For simplicity we have adopted a single time-independent mass distributions for each type of merging binary: BH-BH, BH-NS, and NS-NS. Looking backward to higher redshift, however, the relative proportions of each binary type change, as each possesses a different delay time distribution  $dP/dt$ . In other words, despite using “time-independent” mass distributions, the *instantaneous total mass distribution*, found by gluing these three distributions together in proportion to their instantaneous merger rates  $\mathcal{R}$ , will vary with time. Networks of advanced detectors and particularly third generation detectors will probe a time-dependent mass distribution. The authors and collaborators will also address this issue in a future paper.

## 5. CBC DETECTION RATES AND DETECTION PROBABILITY

### 5.1. CBC Detection Rates for LIGO

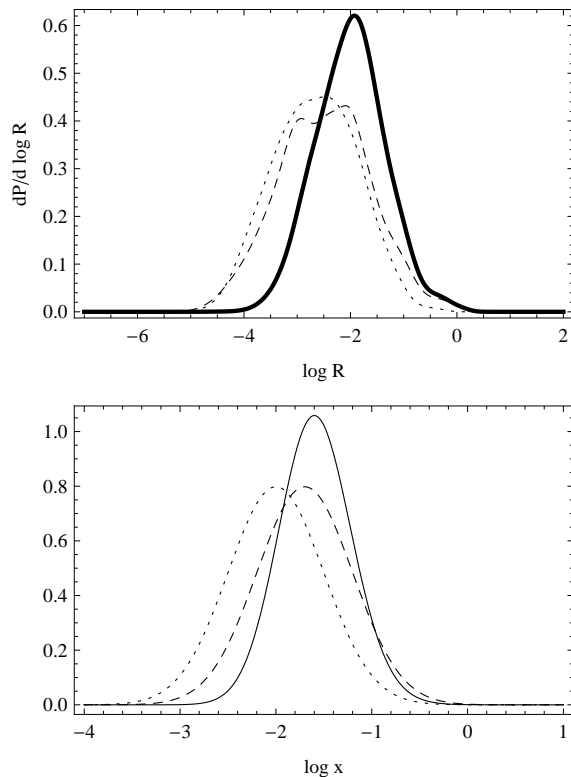


FIG. 6.— Convolutions illustrated. Top panel: the BH-NS merger rates  $\mathcal{R}$  due to ellipticals (dashed), spirals (dotted), and overall (solid) assuming uncorrelated elliptical and spiral star forming conditions, as in the text and Figure 3. The minimum likely merger rate overall is significantly larger than the minimum likely due to ellipticals or spirals alone. Bottom panel: a gaussian distribution  $p(\log x)d \log x$  (dotted);  $p \oplus p$  (solid), analogous to assuming a two-component universe where elliptical and spiral galaxy rates are independently drawn from  $p$ ; and the distribution for  $y = x + x$  (dashed), analogous to a two-component universe with identical elliptical and spiral star forming conditions, both drawn from  $p$ .

Using the `StarTrack` population synthesis code, we have explored a representative sample of stellar evolution produced by elliptical galaxies ( $N_E = 206$ ) and spiral galaxies ( $N_S = 282$ ). From these simulations, using the tools indicated in § 4 we carefully extracted their likely properties (e.g.,  $dP/dt$ ), which in turn we convolved with the star formation history of each of the two major components of the universe (§ 3). Using our understanding of the LIGO range (§ 2) we can convert these merger rate histories into expected single-interferometer LIGO detection rates. Finally, though the set of model universe detection rates  $R_{D,(e,s)k}$  encompasses many of the most significant modeling uncertainties, to be more fully comprehensive and to arrive at a smooth PDF we plot in Figure 7 the convolution of the “model universe” detection rates  $R_{D,s,p}$  and  $R_{D,e,l}$  for  $p = 1, \dots, N_p$  and  $l = 1 \dots N_E$  with the uncertainty kernels and binary fraction kernel described previously assuming equal prior likelihood for

each model (i.e.,  $P(E_l) = 1/N_E$  and  $P(S_p) = 1/N_S$ )

$$\bar{K} = (K_{\text{samp}} * K_{\text{sim}} * K_b) \quad (36)$$

$$p_e(\log R_{D,e}) = \sum_{l=1}^{N_E} P(E_l) \bar{K} \left( \log \frac{R_{D,e}}{R_{D,e,l}} \right) \quad (37)$$

$$p_s(\log R_{D,s}) = \sum_{p=1}^{N_S} P(S_p) \bar{K} \left( \log \frac{R_{D,e}}{R_{D,e,p}} \right) \quad (38)$$

$$p(\log R_D) = (p_e \oplus p_s) \quad (39)$$

and subsequently combine the elliptical and spiral detection rate distributions [Eq. (18)]. [Most of these convolutions can be performed trivially by adding the standard deviations of gaussians in quadrature; the remaining two convolutions are performed numerically.] As previously we estimate the total detection rate via a three-fold convolution [Eq. 32].<sup>21</sup> Though the same basic techniques applied above can be and have been applied to BH-NS and NS-NS binaries previously (PS-GRB), we now incorporate error propagation, a simulation-by-simulation estimate of the relevant chirp mass, and a variable binary fraction; the merger rate distributions they provide therefore are not proportional to our predictions.

Figure 7 shows the distribution of CBC detection rates predicted by Eq. (10) for individual initial LIGO interferometers as part of a network (thin curves) as well as the contribution from elliptical galaxies alone (dashed curves).<sup>22</sup> As indicated by the close proximity of the elliptical and total merger rate distributions, most BH-BH mergers that LIGO detects should be produced in elliptical galaxies. This elliptical bias arises because BH-BH binaries have long delays between their formation and eventual merger; their present-day merger rate is more easily influenced by ancient star formation. On the other hand, the difference between the dashed and thin curves in the bottom left panel indicate that the NS-NS merger rate must be *spiral*-dominated.

Because the initial LIGO detectors essentially probe different-sized volumes of the local universe for each merger type, their detection rate distributions are identical to those of any similar-scale single- or multiple-IFO network, mod a constant horizontal offset determined by the relative increase in volume NS-NS binaries can be seen  $[\log V_{N_S-N_S}/4\pi(14 \text{ Mpc})^3/3]$ . Similarly, because a single advanced LIGO detector’s reach to NS-NS and BH-NS binaries is often not cosmologically significant, weighting over detector and source orientation, our predictions for NS-NS and BH-NS detection rates are identical to those for initial LIGO, mod an offset  $[= \log(197/14)^3 = 3.44]$ . However, the typical range of a single detector to BH-BH binaries *does* extend past  $z \simeq 0.25$ , where the star formation rate is noticeably higher and where cosmological volume and redshift factors become significant. But because of the long delay between BH-BH merger and progenitor birth, the BH-BH merger rate  $R(t)$  generally increases much more slowly

<sup>21</sup> Per the discussion of Footnote 13, this convolution only approximates the true detection rate. In practice, one factor usually dominates the detection rate in each component (e.g., for ellipticals, BH-BH mergers).

<sup>22</sup> The raw and postprocessed data used to create these figures is available from the first author on request.

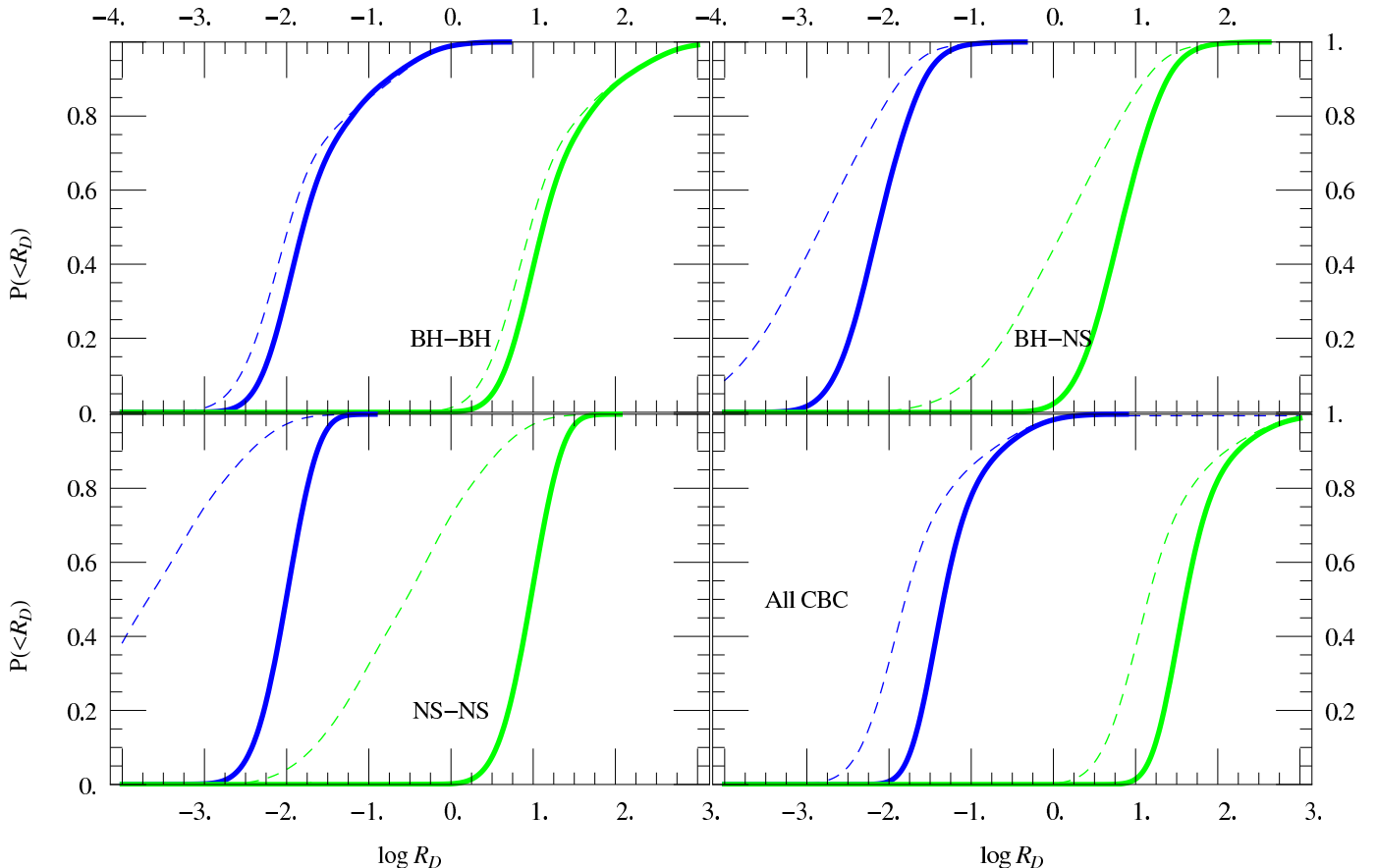


FIG. 7.— Cumulative probability  $P(< \log R_D)$  of various event rates for initial (blue; assuming  $D_H = 31$  Mpc) and advanced (green; assuming  $D_H = 445$  Mpc) single LIGO interferometers as part of a network, requiring consistency with the binary pulsar population in the Milky Way. These distributions incorporate uncertainty in the initial binary fraction, as discussed in the text, as well as uncertainty in the many population synthesis model parameters. For comparison the dashed curves show the contribution from *ellipticals only*.

with redshift than the star formation history. As a result, the single-IFO BH-BH detection rate distribution is also comparable to but slightly less than what we expect after scaling up initial-LIGO results to larger range: a detailed calculation suggests a merger detection rate between  $3 - 300 \text{ yr}^{-1}$  (90% confidence), in good agreement with the  $20 - 500 \text{ yr}^{-1} (D_{\text{bns}}/197 \text{ Mpc})^3$  (90% confidence) expected from cubic rescaling of the initial LIGO result.<sup>23</sup> For networks of advanced detectors, however, cubic scaling breaks down severely; the range is significant enough to require a full cosmological treatment and network-sensitivity-beampattern averaging.

### 5.2. Comparisons with pulsar observations of Galactic NS-NS binaries

Following the previously-discussed procedure to re-evaluate the likelihood of our spiral-galaxy population synthesis models, we arrive at a distribution of initial LIGO detection rates as indicated in Figure 7. Compar-

<sup>23</sup> In our simulations, the black hole-black hole rates generally are *constant* or *decrease* with redshift, due to the long delay between binary birth and merger. Also, the “redshifting factor”  $1+z$  in the detection rate integral implies a slightly smaller comoving 4-volume swept out by the detector’s past light cone per unit time at the maximum redshift:  $\int dz dV_c/dz/(1+z) \simeq V_c/(1+z)$ . Both these factors suggest the BH-BH detection rate at high redshift will be *lower* than a simple cubic extrapolation of the local-universe result.

ing these distributions with the unconstrained results of the previous calculation, we arrive at the following conclusions:

*Higher NS-NS detection rate:* As seen in Figure 3, inferences drawn from the double pulsar population about the present-day NS-NS merger rate lie on the high end of what our models can presently reproduce. By requiring our models reproduce those observations, our constrained distributions naturally favor higher NS-NS detection rates.

*Lower BH-BH detection rate from spirals:* Compared to our previous results (Fig. 7), the highest binary black hole merger and thus detection rates are ruled out *in spiral galaxies*. Physically, the observational constraint supports those population synthesis models where one particular parameter ( $\alpha\lambda$ , related to common-envelope evolution) is not exceptionally small ( $\alpha\lambda > 0.1$ ); see for comparison the top left panel of Figure 5 in PSC2. In turn, this parameter  $\alpha\lambda$  correlates strongly with the BH-BH merger rate, with low values of  $\alpha\lambda$  being required to produce the largest BH-BH merger rates. Thus, because observations of NS-NS binaries in the Milky Way favor high NS-NS merger rates, they disfavor the highest rates of BH-BH mergers in spiral galaxies.

*Observations of the NS-NS merger rate in spiral galaxies do not constrain ellipticals, BH-NS well:* With the exception of NS-NS mergers, Figure 3 demonstrates that most *constrained* predictions for merger rates (and, though not

shown here, LIGO’s detection rate) agree strikingly well with our *a priori* expectations. These consistent predictions should be expected, since observations of spiral galaxies cannot constrain differences (e.g., due to metallicity and IMF) in the binary evolution in elliptical galaxies. In particular, the single most likely source of a gravitational wave detection in the near future, BH-BH mergers, are due to their long characteristic ages expected to occur primarily in elliptical galaxies; as a result, the present-day BH-BH and total CBC detection rate depends only weakly on our ability to rule out certain population synthesis parameters in spiral galaxies. Furthermore, even in spiral galaxies alone, as seen in PSC2 and references therein, the NS-NS and other CBC merger rates are not tightly correlated. Thus despite the fairly strong and consistent constraints that double pulsar observations imply for *binary evolution parameters*, as described in detail in PSC2, our overall expectations for LIGO’s detection rate remain largely unchanged.

### 5.3. Net probability of CBC detection

Factoring in poisson statistics for each model, the net prior probability  $P_d$  that a single LIGO interferometer with a single-IFO range to NS-NS inspiral of  $D_{\text{bns}}$  operating for time  $T$  can make at least one detection is

$$P_{\text{detect}}(\geq 1|D_{\text{bns}}, T) = \int dR_D p(R_D)(1 - e^{-R_D T}) \quad (40)$$

where  $D_{\text{bns}}$  implicitly enters as a scale factor for  $R_D$  ( $\propto D_v^3$ ). More generally, for a multi-interferometer configuration with a time-varying network sensitivity, the appropriate detection probability can be easily calculated from our reference probability by replacing  $T$  in the above expression by  $\int dt (D_{\text{bns}}(t)/D_{\text{bnsref}})^3$ ; the latter quantity characterizes the 4-volume to which the search is sensitive. This detection probability can be significantly increased by improvements in the LIGO detector or run schedule that improve the detection 4-volume  $VT$ . Assuming a fixed, orientation-averaged range  $D_{\text{bns}}$  for any fraction of the whole LIGO network, the total probability of detecting one or more events by that fractional network can be approximated by

$$P_{\text{detect}}(\geq 1|14 \text{ Mpc}, T) \simeq 0.4 + 0.5 \log(T/8 \text{ yr}) \quad (41a)$$

$$P_{\text{detect}}(\geq 1|197 \text{ Mpc}, T) \simeq 0.4 + 0.5 \log(T/0.01 \text{ yr}) \quad (41b)$$

for  $T$  between 1 yr and 100 yr or  $2 \times 10^{-3}$  and 0.1 yr, respectively. These approximations are shown in Figure 8.

Equivalently, our calculations suggest that a gravitational-wave network must have a 4-volume sensitivity of  $1.3 \times 10^5 \text{ Mpc}^3 \text{ yr}$  (roughly equivalent to a 32 Mpc sphere for 1 year) in order to have a 50% chance of detecting one or more events, as

$$P_{\text{detect}}(\geq 1|D_{\text{bns}}, 1 \text{ yr}) \simeq 0.5 + 1.5 \log D_{\text{bns}}/32 \text{ Mpc} \quad (42)$$

for  $D_{\text{bns}}$  between 20 and 70 Mpc.

### 5.4. Comparison to earlier studies

Our fiducial predictions for compact object merger rates [Fig. 3] and gravitational wave detection rates [Fig. 7] reflect our uncertainties about the star-formation conditions and history of the universe. For example, results consistent with current observational constraints

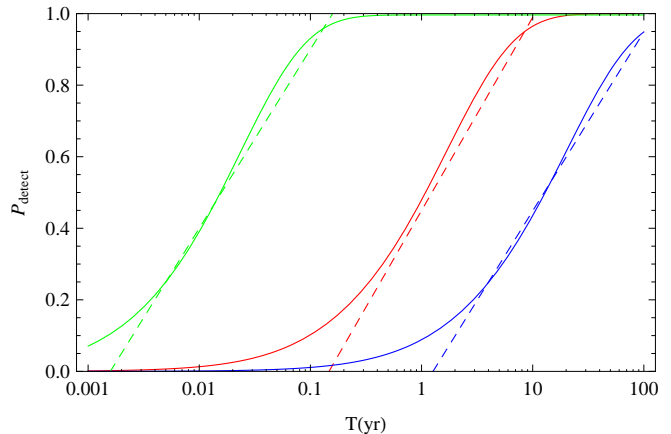


FIG. 8.— Probability  $P_{\text{detect}}(\geq 1|D_{\text{bns}}, T)$  [Eq. (40)] of detecting at least one CBC merger in time  $T$  yr by a single interferometer as part of a network with volume-averaged range  $D_{\text{bns}} = 14$  Mpc (solid blue), 32 Mpc (solid red) and 197 Mpc (solid green) to double-neutron star inspiral, taking into account information about binary pulsars in the Milky Way. For comparison, the dashed curves corresponds to the approximations presented in Eq. 41.

TABLE 1

PARAMETERS OF ALL BINARY EVOLUTION SIMULATIONS USED IN THIS PAPER, ALONG WITH PREDICTED MERGER RATES  $R$ , DETECTION RATES  $R_D$ , AND (FOR SPIRAL SIMULATIONS) POSTERIOR PROBABILITIES. THIS TABLE IS AVAILABLE IN THE ONLINE VERSION OF THE JOURNAL.

require compact binary formation in elliptical galaxies and therefore disallow the worst-case scenario: mergers formed only in spirals by our least-efficient spiral-galaxy model. Nonetheless, our broad parameter study encompasses many scenarios and predictions. For 100% binary fraction and for each type of compact binary (NS-NS, BH-NS, and BH-BH), the most optimistic and pessimistic single-component scenarios in our comprehensive table of results (Table 1, available in the online version of the Journal)<sup>24</sup> correspond to merger rates extending between  $10^{-4} - 1 \text{ Myr}^{-1} \text{ Mpc}^{-3}$ , multiplied by a factor of order unity.

Detailed quantitative comparisons of our results to others appearing in the literature must account for alternate normalization and star formation history choices, which often vary significantly from study to study. Our constant star-formation spiral-galaxy predictions<sup>25</sup> in Table 1 are comparable to Table 4 in the review article by Postnov & Yungelson (2007), to Table I in Belczynski et al. (2002), to Tables 2 and 3 in Belczynski et al. (2007a), and to Table 5

<sup>24</sup> For each simulation used in this study, this table provides input parameters; the number of each type of binary appearing 10 Gyr after a starburst ( $n$  in the appendix); the number of binaries predicted to merge within the age of the universe ( $m$  in the appendix); and, after convolving with a suitable star formation rate, the present-day merger and gravitational-wave detection rate for each binary type.

<sup>25</sup> Most predictions in the literature present results only for the Milky Way, based on an implicit or explicit steady star formation rate assumption. These results can be translated using our present-day spiral-galaxy star formation rate (§3) and the density of Milky Way-equivalent galaxies, by blue luminosity ( $\simeq 0.01 \text{ Mpc}^{-3}$ ); see, e.g., Koppapu et al. (2008).

in Hurley et al. (2002). Our constant star-formation elliptical-galaxy<sup>26</sup> predictions can be compared to Tables 4, 6, and 7 of Voss & Tauris (2003) and to Table 1 in Portegies Zwart & Yungelson (1998). Our results assuming all galaxies have spiral-like star forming conditions [cf. Fig 5] can be compared with Bulik & Belczyński (2003). Finally, our constant and time-dependent elliptical galaxy results are directly comparable to de Freitas Pacheco et al. (2006). Even after allowing for different inputs, a model-by-model comparison of our results with others available in the literature illustrate physical differences between different authors’ population models and our own [§ 4.1]. For example, unlike Voss & Tauris (2003), rather than calculate the envelope binding energy fraction  $\lambda$ , we fix a single factor  $\alpha\lambda$  for all binaries in common envelope, leading to smaller BH-BH merger rates for comparable parameters; see, e.g., the discussion in Postnov & Yungelson (2007). As discussed in §4.6, unlike Postnov & Kuranov (2008) we adopt isotropic kicks, avoiding the least favorable kick configurations and merger rates; see their Figure 3. Unlike model C in Belczynski et al. (2007a), we assumed that the common-envelope evolution of a Hertzsprung gap donor led to stellar merger, not a compact binary. We apply a similar kick to all NS, rather than assign a different kick based on its prior (binary) evolution history (Pfahl et al. 2002) or its supernova mechanism (i.e., a low kick for electron-capture supernova; see Linden et al. (2009), Kalogera et al. (2008) and references therein). Additionally, as described in § 4.1 and § 4.6, we make several other specific choices consistent with our previous work but not universally adopted in the literature (e.g., for the Bondi accretion rate in episodes of hypercritical common envelope accretion; for maximum NS mass). However, a detailed exploration of all these correlated effects would require coordinated simulations performed for the purpose of detailed comparisons; such an undertaking is beyond the scope of this paper. Instead, we are satisfied that our results are broadly consistent with early studies of the Milky Way, particularly given the number and parameter survey breadth of the model database used here compared with earlier studies by other groups. For comparison, in the analysis of our present results we do make detailed comparisons to earlier studies from our group (§ 4.6 and again in our concluding discussion), to make the origin of any apparent inconsistencies fully transparent.

Despite providing a distribution, our fiducial results conservatively do not account for any other channels for forming compact objects besides isolated binary evolution, even though several observational, semianalytic, and numerical studies have demonstrated that interacting stellar environments can efficiently form compact binaries. For example, in young very massive stellar clusters, a high-mass black hole subcluster can mass segregate and rapidly form and eject merging black hole binaries (see, e.g., Portegies Zwart & McMillan (2000);

O’Shaughnessy et al. (2007b); Banerjee et al. (2010) and references therein). A similar process occurs in nuclear star clusters; see Miller & Lauburg (2009). Alternatively, young dense clusters could undergo runaway stellar collisions, eventually forming an “intermediate-mass” black hole  $M \in 100 - 10^3 M_{\odot}$ , each of which can capture stellar-mass compact objects (Mandel et al. 2008) or even form binaries and merge themselves (Fregeau et al. 2006; Mandel et al. 2009). Theory aside, observations suggest pulsar and X-ray binaries are highly overabundant in clusters; see, e.g., Rasio et al. (2000); Pooley et al. (2003); Ransom et al. (2005) and references therein. Further, several authors have argued observations of short GRBs’ hosts, luminosities, and redshift distribution support a multi-component origin, as cluster dynamics lead to a different merger delay-time distribution  $P(> t)$ ; see Hopman et al. (2006), Salvaterra et al. (2007), Guetta & Stella (2009) and references therein. Though present-day massive stellar clusters have little mass, if a sufficient fraction of all star formation occurs through clusters and a sufficient fraction occurs in massive clusters, similar highly efficient dynamical processes could produce many merging compact binaries of all types; see, e.g., Sadowski et al. (2008). To summarize, both theory and several different types of observation suggest that all types of dynamically-produced compact binary merger exist. These mergers could occur as and potentially orders of magnitude more frequently than mergers produced from field binaries; the estimates shown in Fig 7 therefore *underestimate* the total merger rate, summed over all channels. Nonetheless, we anticipate that future observations might distinguish between the relative contributions of each component. Assuming even rough separation, our results determine how and how precisely future measurements of compact object merger rates (through gravitational waves, short GRBs, or galactic observations) will constrain binary evolution.

## 6. CONCLUSIONS AND DISCUSSION

In this paper, we provide the first estimate of the CBC detection rate for initial and advanced LIGO which accounts for (i) star formation in both elliptical and spiral galaxies as a function of redshift, (ii) binary black holes, (iii) a range of plausible binary fractions, and most significantly (iv) a large range of plausible binary evolution scenarios. Our results strongly indicate that that existing gravitational wave detectors are at the threshold of detection; that moderate improvements in these detectors, such as the enhanced LIGO upgrade of 2009, could plausibly lead to detecting at least one binary merger in a year of operation; that advanced LIGO detectors should be reasonably expected to detect inspirals over 1-2 yr of operation; and that even the absence of a detection by advanced interferometers would very significantly constrain the set of model parameters that could be consistent with observations.

Our predicted detection rates are somewhat higher than those presented in PSC2 because we include elliptical galaxies: mergers in elliptical galaxies likely dominate our estimates of the BH-BH and BH-NS event rates. However, our previous estimates effectively assumed a high present-day star formation rate per unit volume: an assumed Milky Way-equivalent galaxy density of  $0.01/\text{Mpc}^3$  and star formation rate per spiral

<sup>26</sup> These papers adopt a Salpeter-like IMF but steady star-formation rate, a combination not provided in our Table 1. For a steady star formation rate, the merger rate can be estimated from two entries in the table: the ratio of the number of merging binaries ( $m$ ) to the star formation time ( $T$ ), corrected for the mass ratio distribution; see the Appendix of O’Shaughnessy et al. (2005).



galaxy of  $3.5M_{\odot}/\text{yr}$  correspond to a present-day star formation rate three times higher than observed. For this reason, a naive product of the merger rates per Milky Way galaxy drawn from PSC2’s Figure 6 leads to preferred merger rates per unit volume that agree well with our preferred values. For example, our current results and this naive rescaling of PSC2 results both favor local merger rate densities of  $10^{-2} \text{Mpc}^{-3} \text{Myr}^{-1}$  for black hole-neutron star binaries and  $3 \times 10^{-2} \text{Mpc}^{-3} \text{Myr}^{-1}$  for binary neutron stars. Correcting for the star formation history normalization, however, our calculations suggest three times as many mergers per volume for BH-NS and NS-NS than in PSC2. Similarly, our predicted detection rates are higher than those implied by Figure 7 in PSC2, correcting for the previously mentioned star formation rate bias (reducing the rates shown in that figure by 3) and rescaling to a single-interferometer rather than network range (reducing the rate by  $\times 10$ ).

Limiting attention to elliptical- plus spiral-galaxy models that include only those spiral galaxy history models that reproduce current observations of double pulsars, we find that a single detector in the initial LIGO network should be sensitive to  $2.4 \times 10^{-2} - 0.46 (\rho_c/8)^{-3} (D_{bns}/14 \text{Mpc})^3$  mergers per year (90% confidence level), where we sum over all merger types to produce an overall detection rate, where  $\rho_c = 8$  is the threshold SNR of the search and  $D_{bns}$  is the radius of the effective volume inside of which a single detector in the appropriate array could observe the inspiral of two  $1.4M_{\odot}$  neutron stars. We estimate that the LIGO detector network has a probability  $P_{\text{detect}}(\geq 1) \geq 0.4 + 0.5 \log(V/V_c)(T/8 \text{yr})$  of detecting a merger during each year of operation, where  $V = 4\pi D_{bns}^3/3$  is the volume to which a multidetector search for binary neutron star inspiral is sensitive,  $V_c$  is the volume inside a 14 Mpc radius sphere, and  $1/3 < (V/V_c)(T/\text{yr}) < 8$ . For example, the probability  $P_{\text{detect}}$  of detecting one or more mergers can be approximated by (i)  $P_{\text{detect}} \simeq 0.4 + 0.5 \log(T/0.01 \text{yr})$ , assuming  $D_{bns} = 197 \text{Mpc}$  and it operates for  $T$  years, for  $T$  between 2 days and 0.1 yr; or by (ii)  $P_{\text{detect}} \simeq 0.5 + 1.5 \log D_{bns}/32 \text{Mpc}$ , for one year of operation and for  $D_{bns}$  between 20 and 70 Mpc.

In this paper we have continued to employ approximate waveform and detection models to estimate the sensitivity of ground-based gravitational wave detectors to moderate-mass ( $M \simeq 10M_{\odot}$ ) BH-BH mergers (see, e.g., Flanagan & Hughes (1998) and Buonanno et al. (2003) for a review). Advanced detectors, however, will be sensitive at cosmological distances to the later phases of high-mass mergers, a complex strong-field and strongly-precessing regime which is only beginning to be thoroughly understood through numerical simulations. Progress in numerical waveform modeling and search pipeline analysis is required to better understand how often these candidates could be identified, especially for spinning systems, as expected in nature.

### 6.1. Anticipated constraints from future observations

Despite the existence of two competing scenarios for compact binary formation, in many cases the electromagnetic and gravitational wave signatures of binaries formed dynamically and in isolation can be distinguished. For example, black hole binaries formed dynam-

ically should have random spins and therefore (generically) beating gravitational inspiral waveforms, while isolated binary evolution models favor spin-orbit alignment. Once binaries with isolated progenitors are identified, their gravitational wave signals will encode both the number and properties of binaries formed through isolated evolution, information that in turn can tightly constrain isolated binary progenitor parameters. To use an extreme example, future BH-BH observations could imply a gravitational-wave detection rate  $R_D$  consistent with only the highest event rates shown in Fig. 7. In the context of the models presented here, such an observation would imply (i) that elliptical galaxies host most BH-BH binaries; (ii) that massive stars have a high binary fraction; (iii) that a certain phenomenological parameter is very small ( $\alpha\lambda < 0.1$ ; §5.2); and thus (iv) since Milky Way observations of binary pulsars exclude low  $\alpha\lambda$ , that isolated binaries formed in elliptical galaxies evolve differently to those in spirals. However, by analogy with the insights provided from observations of isolated Galactic pulsars, typical detection rates will be compatible with many plausible progenitor models; see PSC2 and O’Shaughnessy et al. (2005). Rather than constraining single parameters tightly, the information provided by the first few observations will be encoded only in high-order correlations among many model parameters; see, e.g., Fig. 5 in PSC2 and the highly correlated merger rate fit presented in Appendix B in O’Shaughnessy et al. (2005). Finally, what we can learn about binary evolution depends on the merger detections that nature provides. Because correlations between parameters change significantly across the model space, we cannot describe posterior uncertainties once and for all.

If neutron star mergers occasionally have electromagnetic counterparts (i.e., short GRBs), then well-localized electromagnetic counterparts to binary neutron star mergers, such as (prompt or orphan) short GRB afterglows Gehrels et al. (2009); Rau et al. (2009); Bloom & et al (2009) or radio bursts, allow optical follow-up studies of its host galaxy’s star-forming and chemical enrichment history. Combined with the position of the burst on the galaxy (kick) and, if within range of gravitational wave detectors, the binary component masses, this host information can tightly limit isolated binary progenitor models; see, e.g., PS-GRB. For example, these observations could provide unique direct probes on the distribution of delays between binary birth and merger; see, e.g., Nakar (2007), Prochaska et al. (2006), Zheng & Ramirez-Ruiz (2007), Rhoads (2010) and references therein. Better still, offsets from host galaxies might provide an independent constraint on delay times (and on supernova kick velocities); see, e.g., Belczynski et al. (2006), Troja et al. (2008) and references therein. Unfortunately, purely electromagnetic observations of short GRBs cannot distinguish between multiple source populations, such as cluster-formed mergers or even non-merger-powered bursts (see, e.g. Virgili et al. 2009; Chapman et al. 2008). Worse, given plausible kick offsets, purely electromagnetic observations may not isolate the appropriate host (Zemp et al. 2009). Fortunately, if existing space-based and ground-based resources are applied in the advanced LIGO epoch, coincident gravitational-wave and electromagnetic observations can resolve these ambiguities.

Finally, as always with binary evolution, any further observations pertaining to binary stars can improve our understanding and limit model-building freedom, such as SNIa rates; galactic pulsar and X-ray binaries; and even galactic WD binaries [see, e.g., the extensive discussion in Nelemans & et al (2009)].

The authors appreciate helpful comments received from Ilya Mandel, Alberto Vecchio, Patrick Brady, Chad Hanna, Steve Fairhurst, Tania Regimbau, Alan Weinstein, and all the members of LIGO inspiral search group. **Grants** R.O. was supported by National Science Foundation awards PHY 06 -53462 and the Center for Gravitational Wave Physics. The Center for Gravitational

Wave Physics is supported by the George A. and Margaret M. Downsbrough Endowment and by the National Science Foundation under cooperative agreement PHY 01-14375. VK was supported by NSF grant PHY-0653321. KB acknowledges the support from the Polish Ministry of Science and Higher Education (MSHE) grant N N203 302835 (2008-2011).

## REFERENCES

- Abbott et al. (The LIGO Scientific Collaboration). 2003, (gr-qc/0308043) [URL]  
 —. 2006, *Phys. Rev. D*, 73, 062001 [ADS]  
 —. 2008, *Phys. Rev. D*, 77, 062002 [URL]  
 Abbott et al. (The LIGO Scientific Collaboration), B. 2009, *Phys. Rev. D*, 79, 122001 [ADS] [ADS]  
 Acernese, F., Amico, P., Alshourbagy, M., Antonucci, F., Aoudia, S., Avino, S., Babusci, D., Ballardín, G., Barone, F., Barsotti, L., Barsuglia, M., Beauville, F., Bigotta, S., Birindelli, S., Bizouard, M. A., Boccara, C., Bondu, F., Bosi, L., Bradaschia, C., Braccini, S., Brillet, A., Brissou, V., Brocco, L., Buskulic, D., Calloni, E., Campagna, E., Cavalieri, F., Cavalieri, R., Cella, G., Cesarini, E., Chassande-Mottin, E., Corda, C., Cottone, F., Clapson, A.-C., Cleva, F., Coulon, J.-P., Cuoco, E., Dari, A., Dattilo, V., Davier, M., DeRosa, R., Di Fiore, L., Di Virgilio, A., Dujardin, B., Eleuteri, A., Enard, D., Ferrante, I., Fidecaro, F., Fiori, I., Flaminio, R., Fournier, J.-D., Francois, O., Frasca, S., Frasconi, F., Freise, A., Gammaitoni, L., Garufi, F., Gennai, A., Giazotto, A., Giordano, G., Giordano, L., Gouaty, R., Grosjean, D., Guidi, G., Hebri, S., Heitmann, H., Hello, P., Holloway, L., Karkar, S., Kreckelbergh, S., La Penna, P., Laval, M., Leroy, N., Letendre, N., Lorenzini, M., Lorette, V., Loupias, M., Losurdo, G., Mackowski, J.-M., Majorana, E., Man, C. N., Mantovani, M., Marchesoni, F., Marion, F., Marquet, J., Martelli, F., Masserot, A., Mazzoni, M., Milano, L., Moins, C., Moreau, J., Morgado, N., Mours, B., Pai, A., Palomba, C., Paoletti, F., Pardi, S., Pasqualetti, A., Passaquieti, R., Passuello, D., Perniola, B., Piergiovanni, F., Pinard, L., Poggiani, R., Punturo, M., Puppo, P., Qipiani, K., Rapagnani, P., Reita, V., Remillieux, A., Ricci, F., Ricciardi, I., Ruggi, P., Russo, G., Solimeno, S., Spallicci, A., Stanga, R., Taddei, R., Tonelli, M., Toncelli, A., Tournefier, E., Travasso, F., Vajente, G., Verkindt, D., Vetrano, F., Viceré, A., Vinet, J.-Y., Vocca, H., Yvert, M., & Zhang, Z. 2006, *Classical and Quantum Gravity*, 23, 635 [ADS]  
 Adhikari, R., González, G., Landry, M., O'Reilly, B., & the LIGO Scientific Collaboration. 2003, *Classical and Quantum Gravity*, 20, 903 [ADS]  
 Ajith, P., Hannam, M., Husa, S., Chen, Y., Bruegmann, B., Dorband, N., Mueller, D., Ohme, F., Pollney, D., Reisswig, C., Santamaria, L., & Seiler, J. 2009, (arXiv:0909.2867) [URL]  
 Anderson, W. G., Whelan, J. T., Brady, P. R., Creighton, J. D. E., Chin, D., & Riles, K. 2001, *Beam Pattern Response Functions and Times of Arrival for Earthbound Interferometers*, Tech. Rep. LIGO-T010110-00-Z, LIGO Project [URL]  
 Apostolatos, T. A., Cutler, C., Sussman, G. J., & Thorne, K. S. 1994, *Phys. Rev. D*, 49, 6274 [ADS]  
 Banerjee, S., Baumgardt, H., & Kroupa, P. 2010, *MNRAS*, 402, 371 [URL] [ADS]  
 Belczynski, K., Bulik, T., Fryer, C. L., Ruiter, A., Vink, J. S., & Hurley, J. R. 2009, ArXiv e-prints [ADS]  
 Belczynski, K., Hartmann, D. H., Fryer, C. L., Holz, D. E., & O'Shea, B. 2008a, ArXiv e-prints [ADS]  
 Belczynski, K., Kalogera, V., & Bulik, T. 2002, *ApJ*, 572, 407 [ADS]  
 Belczynski, K., Kalogera, V., Rasio, F., Taam, R., Zezas, A., Maccarone, T., & Ivanova, N. 2008b, *ApJS*, 174, 223 [URL] [ADS]  
 Belczynski, K., Perna, R., Bulik, T., Kalogera, V., Ivanova, N., & Lamb, D. Q. 2006, *ApJ*, 648, 1110 [ADS]  
 Belczynski, K., Taam, R. E., Kalogera, V., Rasio, F. A., & Bulik, T. 2007a, *ApJ*, 662, 504+ [ADS]  
 Belczynski, K., Taam, R. E., Rantsiou, E., & Sluys, M. v. d. 2007b, submitted to *ApJ* (astro-ph/0703131) [URL]  
 Bloom, J. S. & et al. 2009, ArXiv e-prints [ADS]  
 Brown, D. 2004, Ph.D. Thesis, U. Wisconsin at Milwaukee [URL]  
 Brown, G. E. & Bethe, H. A. 1994, *ApJ*, 423, 659 [ADS]  
 Bulik, T. & Belczyński, K. 2003, *ApJ*, 589, L37 [ADS]  
 Bulik, T., Belczynski, K., & Prestwich, A. 2008, (arXiv:0803.3516) [URL]  
 Bulik, T., Gondek-Rosinska, D., & Belczynski, K. 2004, *MNRAS*, 352, 1372 [ADS]  
 Buonanno, A., Chen, Y., & Vallisneri, M. 2003, 67, 104025 [URL]  
 Buonanno, A., Chen, Y., & Vallisneri, M. 2003, *Phys. Rev. D*, 67, 104025 [ADS]  
 Chapman, R., Priddey, R. S., & Tanvir, N. R. 2008, (arXiv:0802.0008) [URL]  
 Cutler, C. & Flanagan, E. 1994, *Phys. Rev. D*, 49, 2658 [ADS]  
 de Freitas Pacheco, J. A., Regimbau, T., Vincent, S., & Spallicci, A. 2006, *International Journal of Modern Physics D*, 15, 235 [ADS] [ADS]  
 de Mink, S. E., Cantiello, M., Langer, N., Pols, O. R., Brott, I., & Yoon, S.-C. 2009, *A&A*, 497, 243 [ADS]  
 Duquennoy, A. & Mayor, M. 1991, *A&A*, 248, 485 [ADS]  
 Fall, S. M., Chandar, R., & Whitmore, B. C. 2005, *ApJ*, 631, L133 [ADS]  
 Finn, L. S. & Chernoff, D. F. 1993, *Phys. Rev. D*, 47, 2198 [ADS]  
 Flanagan, É. É. & Hughes, S. A. 1998, *Phys. Rev. D*, 57, 4535 [ADS]  
 Fregeau, J. M., Larson, S. L., Miller, M. C., O'Shaughnessy, R., & Rasio, F. A. 2006, *ApJ*, 646, L135 [ADS] [ADS]  
 Fryer, C., Burrows, A., & Benz, W. 1998, *ApJ*, 496, 333 [ADS]  
 Fryer, C. L., Woosley, S. E., & Hartmann, D. H. 1999, *ApJ*, 526, 152 [ADS]  
 Gallagher, III, J. S., Hunter, D. A., & Tutukov, A. V. 1984, *ApJ*, 284, 544 [ADS]  
 Gehrels, N., Ramirez-Ruiz, E., & Fox, D. B. 2009, *ARA&A*, 47, 567 [ADS]  
 Guetta, D. & Stella, L. 2009, *A&A*, 498, 329 [ADS]  
 Hopman, C., Guetta, D., Waxman, E., & Portegies Zwart, S. 2006, *ApJ*, 643, L91 [ADS]  
 Hurley, J. R., Tout, C. A., & Pols, O. R. 2002, *MNRAS*, 329, 897 [ADS]  
 Kalogera, V., Valsecchi, F., & Willems, B. 2008, in *American Institute of Physics Conference Series*, Vol. 983, 40 Years of Pulsars: Millisecond Pulsars, Magnetars and More, ed. C. Bassa, Z. Wang, A. Cumming, & V. M. Kaspi, 433-441  
 Kennicutt, Robert C., J. 1998, *Annual Review of Astronomy and Astrophysics*, 36, 189 [URL]  
 Kopparapu, R. K., Hanna, C. R., Kalogera, V., O'Shaughnessy, R., Gonzalez, G., Brady, P. R., & Fairhurst, S. 2008, *ApJ*, 675, 1459 [URL] [ADS]  
 Kroupa, P. & Weidner, C. 2003, *ApJ*, 598, 1076 [URL]  
 Kulczycki, K., Bulik, T., Belczyński, K., & Rudak, B. 2006, *A&A*, 459, 1001 [ADS]  
 Kuranov, A. G., Popov, S. B., & Postnov, K. A. 2009, *MNRAS*, 395, 2087 [ADS]  
 Li, Z., Zhang, F., & Han, Z. 2006, accepted for publication to *ChJAA* (astro-ph/0605610) [URL]  
 Linden, T., Sepinsky, J. F., Kalogera, V., & Belczynski, K. 2009, *ApJ*, 699, 1573 [ADS]

- M. Landry (for the LIGO Scientific Collaboration). 2005, Classical and Quantum Gravity, 22, S985 [URL]
- Maeder, A. & Meynet, G. 2001, A&A, 373, 555 [ADS]
- Mandel, I., Brown, D. A., Gair, J. R., & Miller, M. C. 2008, ApJ, 681, 1431 [ADS]
- Mandel, I., Gair, J. R., & Miller, M. C. 2009, ArXiv e-prints [ADS]
- Miller, M. C. & Lauburg, V. M. 2009, ApJ, 692, 917 [ADS]
- Nagamine, K., Ostriker, J. P., Fukugita, M., & Cen, R. 2006, ApJ, 653, 881 [URL] [ADS]
- Nakar, E. 2007, Phys. Rep., 442, 166 [ADS]
- Nelemans, G. & et al. 2009, in Astronomy, Vol. 2010, AGB Stars and Related Phenomena 2010: The Astronomy and Astrophysics Decadal Survey, 221–+
- O’Shaughnessy, R., Kalogera, V., & Belczynski, C. 2008a, ApJ, 675, 566+ [URL]
- O’Shaughnessy, R., Kalogera, V., & Belczynski, K. 2007a, ApJ, 667, 1048 [URL]
- O’Shaughnessy, R., Kim, C., Fragos, T., Kalogera, V., & Belczynski, K. 2005, ApJ, 633, 1076 [ADS] [ADS]
- O’Shaughnessy, R., Kim, C., Kalogera, V., & Belczynski, K. 2008b, ApJ, 672, 479 [URL]
- O’Shaughnessy, R., Koppurapu, R., & Belczynski, K. 2008c, submitted to ApJ; arXiv:0812.0591 [URL]
- O’Shaughnessy, R., O’Leary, R., & Rasio, F. A. 2007b, Phys. Rev. D, 76, 061504 [URL]
- Peters, P. 1964, Physical Review, 136, 1224 [ADS]
- Pfahl, E., Rappaport, S., Podsiadlowski, P., & Spruit, H. 2002, ApJ, 574, 364 [ADS]
- Pooley, D., Lewin, W. H. G., Anderson, S. F., Baumgardt, H., Filippenko, A. V., Gaensler, B. M., Homer, L., Hut, P., Kaspi, V. M., Makino, J., Margon, B., McMillan, S., Portegies Zwart, S., van der Klis, M., & Verbunt, F. 2003, ApJ, 591, L131 [ADS]
- Portegies Zwart, S. F. & McMillan, S. L. W. 2000, Astrophysical Journal, 528, L17 [URL]
- Portegies Zwart, S. F. & Yungelson, L. R. 1998, A&A, 332, 173 [ADS]
- Postnov, K. & Yungelson, L. 2007, (astro-ph/0701059) [URL]
- Postnov, K. A. & Kuranov, A. G. 2008, MNRAS, 384, 1393 [URL] [ADS]
- Prochaska, J. X., Bloom, J. S., Chen, H.-W., Foley, R. J., Perley, D. A., Ramirez-Ruiz, E., Granot, J., Lee, W. H., Pooley, D., Alatalo, K., Hurley, K., Cooper, M. C., Dupree, A. K., Gerke, B. F., Hansen, B. M. S., Kalirai, J. S., Newman, J. A., Rich, R. M., Richer, H., Stanford, S. A., Stern, D., & van Breugel, W. J. M. 2006, ApJ, 642, 989 [ADS]
- Ransom, S. M., Hessels, J. W. T., Stairs, I. H., Freire, P. C. C., Camilo, F., Kaspi, V. M., & Kaplan, D. L. 2005, Science, 307, 892 [ADS]
- Rasio, F. A., Pfahl, E. D., & Rappaport, S. 2000, ApJ, 532, L47 [ADS]
- Rau, A., Kulkarni, S. R., Law, N. M., Bloom, J. S., Ciardi, D., Djorgovski, G. S., Fox, D. B., Gal-Yam, A., Grillmair, C. C., Kasliwal, M. M., Nugent, P. E., Ofek, E. O., Quimby, R. M., Reach, W. T., Shara, M., Bildsten, L., Cenko, S. B., Drake, A. J., Filippenko, A. V., Helfand, D. J., Helou, G., Howell, D. A., Poznanski, D., & Sullivan, M. 2009, (arXiv:0906.5355) [URL]
- Rhoads, J. E. 2010, ApJ, 709, 664 [ADS]
- Sadowski, A., Belczynski, K., Bulik, T., Ivanova, N., Rasio, F. A., & O’Shaughnessy, R. 2008, ApJ, 676, 1162 [ADS]
- Salvatera, R., Cerutti, A., Chincarini, G., Colpi, M., Guidorzi, C., & Romano, P. 2007, (arXiv:0710.3099) [URL]
- The VIRGO project website. ??? [URL]
- Troja, E., King, A. R., O’Brien, P. T., Lyons, N., & Cusumano, G. 2008, MNRAS, 385, L10 [ADS]
- Virgili, F. J., Zhang, B., O’Brien, P., & Troja, E. 2009, (arXiv:0909.1850) [URL]
- Voss, R. & Tauris, T. M. 2003, Monthly Notices of the Royal Astronomical Society, 342, 1169 [URL]
- Wang, C., Lai, D., & Han, J. L. 2007, ApJ, 656, 399 [ADS]
- Zemp, M., Ramirez-Ruiz, E., & Diemand, J. 2009, ApJ, 705, L186 [ADS]
- Zhang, Q. & Fall, S. M. 1999, Astrophysical Journal, 527, L81 [URL]
- Zheng, Z. & Ramirez-Ruiz, E. 2007, ApJ, 665, 1220 [URL] [ADS]

## APPENDIX

## RECONSTRUCTING THE MASS AND TIME DISTRIBUTIONS

*Selecting binaries for mass estimation:* We prefer to smooth  $dP/dt$  over a shorter timescale than the maximum allowed by evolution of isolated BH-BH binaries. On physical grounds, double BH binaries whose delay times are comparable to or smaller than the age of the universe are more likely to be similar to merging BH-BH binaries (the focus of our study) than wide binaries that have never interacted. To quantify the point at which the transition occurs and therefore the timescale inside of which BH-BH binaries are comparatively similar, we calculate the “average” chirp mass of binaries  $\bar{\mathcal{M}}_c(t)$  merging within a factor 10 of time  $t$ :

$$\bar{\mathcal{M}}_c(t) = \left[ \frac{\sum_{j:0.1t < t_j < 10t} \mathcal{M}_{c_j}^{15/6}}{\sum_{j:t0.1 < t_j < t10} 1} \right]^{6/15} \quad (\text{A1})$$

Figure 9 shows the results of this calculation. Based on the delay time distribution  $P_m(< t)$  and average chirp mass of similar binaries  $\bar{\mathcal{M}}_c(t)$ , a sharp distinction exists between binaries with  $t \lesssim 10^7$  Myr and wider binaries. These massive wide binaries have orbits largely unaffected by binary evolution and have a delay time distribution  $dP/dt \propto 1/t$  largely determined by their initial orbital configuration. On the contrary, tighter and less massive binaries have been significantly perturbed by binary evolution. Within each simulation, they appear to be drawn from a similar chirp mass distribution (allowing for significant sampling-induced fluctuations in  $\bar{\mathcal{M}}_c(t)$ )

*Predictions and smoothing: Physical timescales* From the above similarity argument, we suspect the  $n_{eff}$  BH-BH binaries with delay times  $t < 10^5$  Myr are similar to the set of binaries with delay times  $< 13.5$  Gyr. However, even with those binaries we often have only  $\sim 50$  with which to estimate  $p(\mathcal{M}_c)$ ; the chirp mass distribution must be estimated with smoothing. We use the same approach as is used for  $dP/dt$  in PS-GRB to estimate the chirp mass

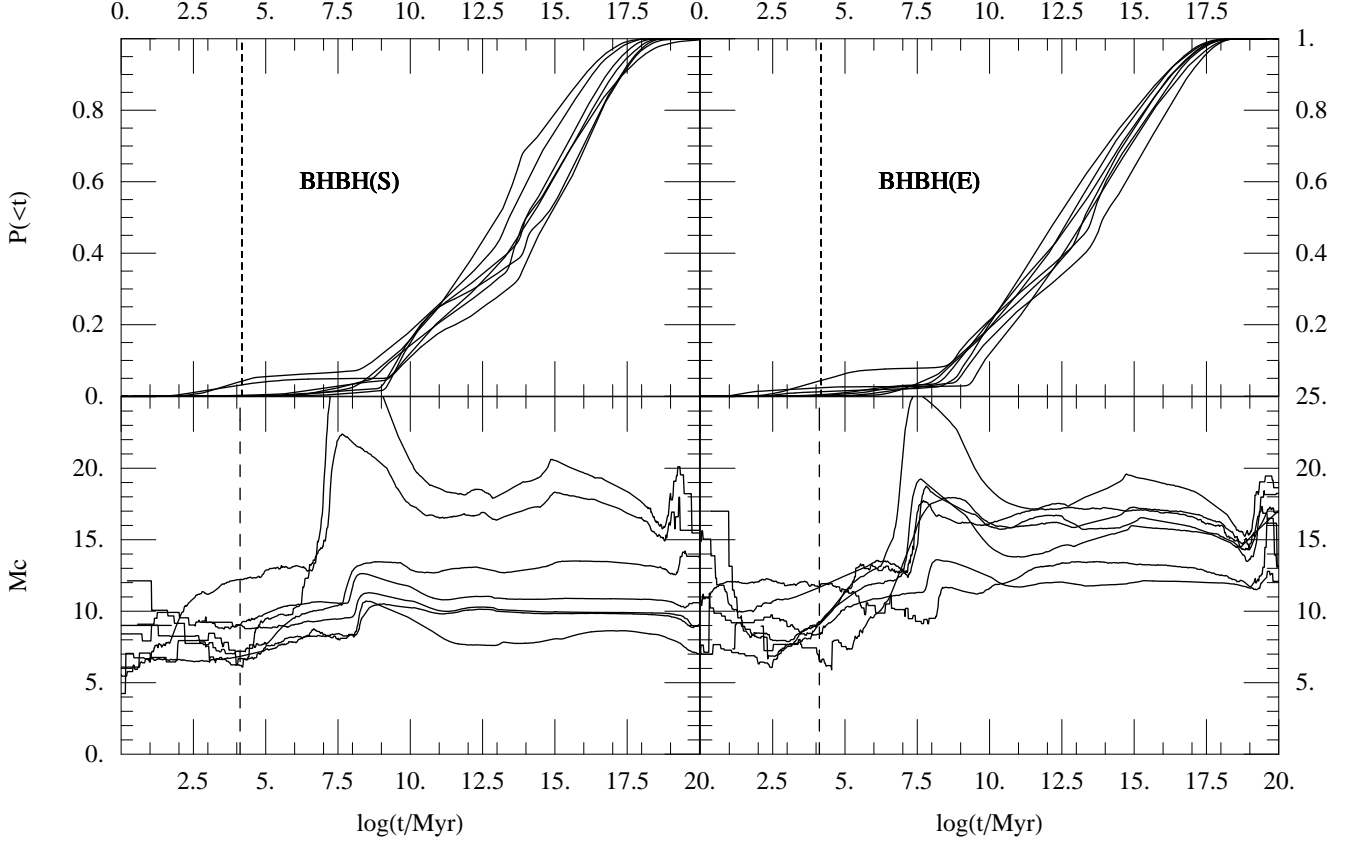


FIG. 9.— Top panels: Cumulative probabilities  $P_m(<t)$  that a BH-BH binary will merge in time less than  $t$ , for **ten** randomly-chosen population synthesis models that satisfy the limitations discussed in the text, given spiral (left) and elliptical (right) star forming conditions. A vertical dashed line indicates the age of the universe. Given the enormous sample sizes involved – by construction, each sample has at least 3000 binaries – these distributions are expected accurate to within **0.03** almost everywhere (with 90% probability), barring the fine details near the short-time and long-time limits. Bottom panels: Average chirp mass  $\bar{M}_c(t)$  [Eq. (A1)] of binaries merging between  $0.1t$  and  $10t$ , versus time. Usually, the binaries that merge within 100 Gyr after their birth have a chirp mass lower than  $10M_\odot$ , significantly lower than the average chirp mass of more separated holes.

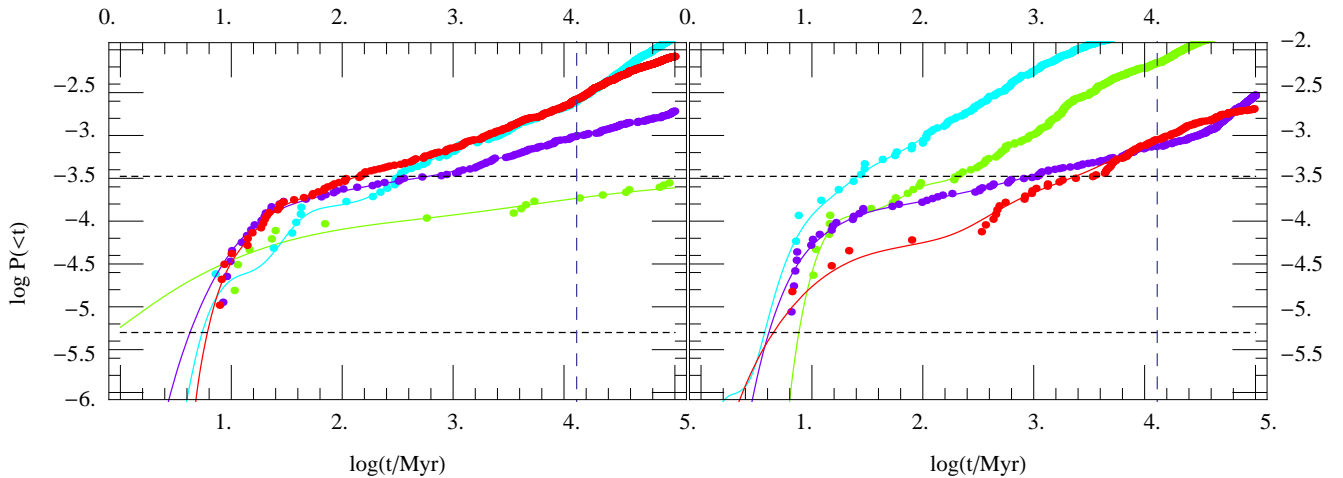


FIG. 10.— Detailed view of the cumulative probabilities  $P_m(<t)$  for 4 randomly selected spiral (left) and elliptical (right) models versus  $\log t/\text{Myr}$ ; compare with Figure 9. Solid curves indicate the fit; points indicate the raw cumulative  $P_m(<t)$ . The horizontal dashed lines indicate the smallest and largest possibilities for  $\log P \approx \log 1/n$ , the smallest resolvable cumulative probability; see Figure 11 and the associated text for a discussion of its range and relation to  $m$  (i.e., the largest  $1/n$  occurs in only a handful of simulations, most of which have many merging binaries  $m \gg 1$  and therefore a well-resolved  $P(<t)$ ). Our estimate reproduces  $P_m(<t)$  reliably at  $t \simeq 100$  Myr, the smallest scale on which  $\rho(t)$  varies for the redshift range of interest. Though our fits necessarily fail to reliably recover  $dP_m/dt$  on very short timescales, uncertainty in integrals of  $dP_m/dt$  over longer timescales average out (i.e., in merger rate estimates  $\mathcal{R}(t)$  using Eq. 15)

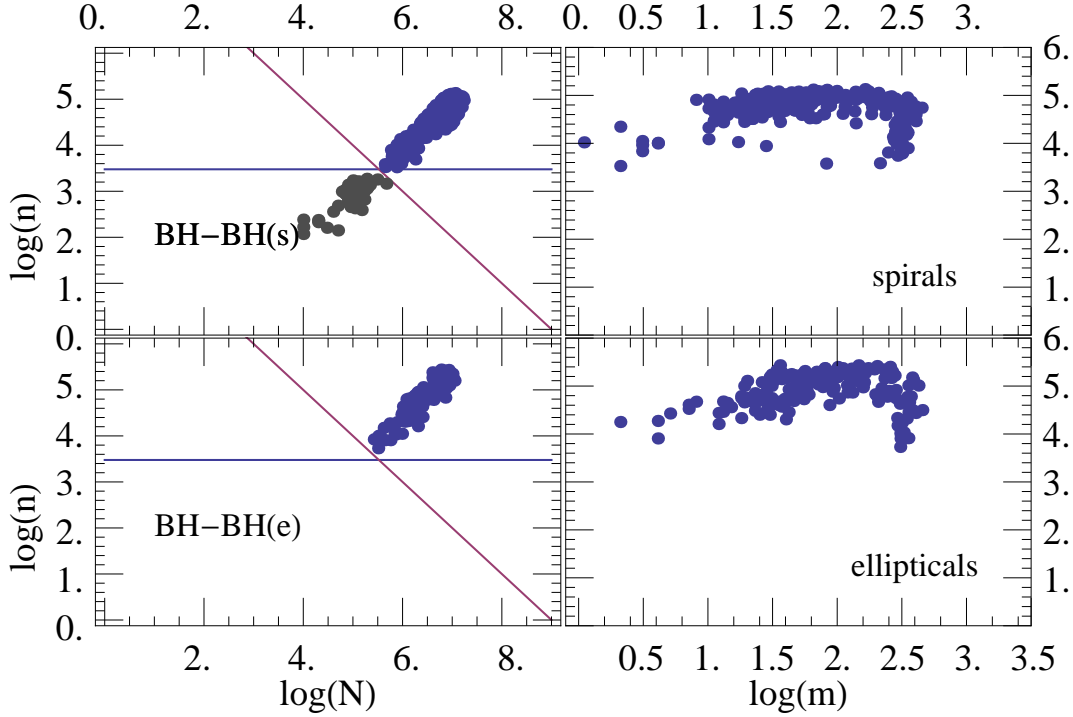


FIG. 11.— Left plot: For spiral (top panels) and elliptical (bottom) archives, a scatter plot of the number of BH-BH binaries  $n$  seen in a simulation of  $N$  progenitor binaries (each progenitor component having mass greater than  $4M_{\odot}$ ; higher primary masses are drawn from the broken-Kroupa IMF). The two solid lines show the cutoffs  $n > 3000$  and  $nN > 1 \times 10^9$  imposed to insure data quality and reduce sampling bias. Simulations used in this paper, shown in blue, must lie above and to the right of these cutoffs. Right plot: For the simulations above and to the right of the lines shown to left, scatter plot of the total number of bound BH-BH binaries remaining in the simulation ( $n$ ) versus the number  $m$  of *potentially-merging binaries* (i.e., with a delay between birth and merger less than 13.5 Gyr). All selected simulations ( $nN > 1 \times 10^9$ ) have at least one merger ( $m > 0$ ).

distribution:

$$\hat{p}(\mathcal{M}_c) \equiv \frac{1}{\mathcal{M}_c n_{eff} \ln 10} \sum_{k=1}^{n_{eff}} \frac{1}{\sqrt{2\pi(s_2)^2}} e^{-(\log \mathcal{M}_c - l_{m,k})^2 / 2(s_2)^2} \quad (\text{A2})$$

$$s_2 \equiv \frac{[(\max_k l_{m,k}) - (\min_k l_{m,k})]}{1.25 \sqrt{n_{eff}}} \quad (\text{A3})$$

where the  $l_{m,k} = \log_{10}(\mathcal{M}_c / M_{\odot})$  for  $k = 1 \dots n_{eff}$  are the logarithms of each binaries' chirp mass for the  $n_{eff}$  binaries with delay times  $< 10^5$  Myr.

*Absent correlations:* We identify very few significant correlations on the timescales of interest between  $\log \mathcal{M}_c$  and  $\log t$ . For example, the correlation coefficient between  $\log \mathcal{M}_{ck}$  and  $\log t_k$  for each simulation's  $n_{eff}$  close BH-BH binaries is roughly consistent with sampling error ( $\propto 1/\sqrt{n_{eff}}$ ). For BH-NS and particularly NS-NS, nominally significant correlation coefficients occur. For example, some NS-NS  $(\mathcal{M}_c, t)$  distributions concentrate a fraction of mergers on and exclude a region below a critical  $t(\mathcal{M}_c)$  curve, associated with mass-transfer-limited ultracompact mergers on times  $t \leq 100$  Myr. Other distributions show no apparent structure, but through large  $n_{eff}$  and therefore extremely narrow mass distributions yield nominally significant correlation. Our manual inspection of all these outliers suggests no structure significant enough to impact merger rates (i.e., associated both with significant change in  $\mathcal{M}_c$  and long star formation timescales). On the contrary, as seen in Figure 9, the joint distribution  $p(\mathcal{M}_c, t)$  varies significantly between simulations, as the distribution in *each factor* [ $\mathcal{M}_c$  and  $t$ ] changes significantly. The authors can provide all binary properties  $[(m_1, m_2, t)]$  for each simulation on request.

### SAMPLING LIMITATIONS AND ARCHIVE SELECTION

Both sets of simulations are highly heterogeneous: the number of binaries simulated ( $N$ ), the number of bound BH-BH binaries remaining at the end of stellar evolution ( $n$ ), and the number of those binaries which merge within 13.5 Gyr ( $m$ ) all span several orders of magnitude, as shown in Figure 11. Evidently, only for those simulations with *many*

BH-BH binaries ( $n \gg 1000$ ) – particularly with several *merging* binaries ( $m \gg 1$ ) – can we reliably extract relevant physics, such as the present-day merger rate and characteristic chirp mass of BH-BH binaries due to a starburst in the early universe. However, as discussed in PS-GRB, the obvious subsets of simulations for which we can reliably make predictions, such as the set of simulations with  $n > 3000$ , could have been biased, over-representing those simulations which predict more mergers per simulated binary. To mitigate the influence of this bias, in *addition* to requiring that each simulation have many BH-BH binaries ( $n > 3000$ ), we also (or, equivalently, instead) require that  $nN > 1 \times 10^9$ . The second cut’s prefactor ( $1 \times 10^9$ ) is chosen so that every simulation that satisfies it has  $n > 3000$ . The subset of simulations which satisfies both conditions has a relatively unbiased distribution of  $n/N$ , the fraction of simulated binaries that end up as bound BH-BH binaries (PS-GRB). These two cuts do not introduce biases in any of the parameters: the set of simulations which satisfy these cuts has similar statistical properties as the entire archive (we omit the many plots needed as proof).

*Handling undersampled cases:* Finally, with each simulation guaranteed to have 3000 binaries, most simulations have a minimum of  $\sim 1$  *merging* BH-BH binaries; see Figure 11 for details. Some simulations still do contain very few binaries that are merging or even nearly so, largely because certain combinations of physical circumstances rarely lead to the formation of many tight black hole binaries. Given that we construct model universes from independent elliptical and spiral simulations, these simulations will lead to an indeterminate, small detection rate in only  $1/N_E N_S \simeq 1/300^2$  universe models, multiplied by a factor of order unity. Even considering only elliptical or spiral galaxy star formation, they influence our predictions  $O(1/N_{E,S}) \simeq 1\%$  of the time, multiplied by a factor of order unity. We therefore adopt a few percent as the lowest resolvable probability of any event our simulations can resolve.

*Potential biases in multiply-selected simulations:* Just as the set of simulations was reduced to find simulations with many BH-BH binaries in § 4, here we require our simulations *additionally* have enough NS-NS binaries to enable accurate estimates.<sup>27</sup> Most population synthesis simulations we performed that produce an adequate number of BH-BH binaries also produce more than enough NS-NS and NS-BH binaries ( $\sim 10^4$ ) to allow us to estimate the three properties ( $\lambda, dP/dt, p(\mathcal{M}_c)$ ) needed to reconstruct merger and detection rates for these NS binaries. However, certain combinations of population synthesis parameters strongly favor merging BH-BH production over NS-NS production. Most of our simulations of these conditions did not produce enough NS-NS binaries to allow accurate estimates. In other words, the set of simulations that have *both* enough NS-NS and close BH-BH binaries is slightly biased against the highest BH-BH and lowest NS-NS merger rates; see Table 1.

The goal of this paper is to determine the relative likelihood of CBC merger and detection rates given existing observations. In particular, in § 5.2 we examine the distribution of BH-BH merger rates for (spiral-galaxy) simulations for which the NS-NS merger rates are consistent with milky Way observations. This subset of simulations is inevitably contained within the biased set of simulations for which NS-NS and BH-BH merger rates can be accurately estimated. That being said, the observational constraints reviewed in § 5.2 point to a high NS-NS merger rate and will therefore inevitably rule out the few models for which NS-NS merger rates could not be accurately determined.

<sup>27</sup> We adopt the same conditions on  $n$  and  $N$  as were used in